(3) W. McFarlane, *Q. Rev., Chem. Soc.*, **23**, 187 (1969).
(4) J. A. Pople, D. P. Santry, and G. A. Segal, *J. Chem. Phys.*, **43**, S129 (1965); J. A. Pople and G. A. Segal, *ibid.*, **43**, S136 (1965); **44**, 3289 (1966).
(5) J. A. Pople and D. L. Beveridge, "Approximate Molecular Orbital Theory", McGraw-Hill, New York, N.Y., 1970.
(6) J. A. Pople, D. L. Beveridge, and P. A. Dobosh, *J. Chem. Phys.*, **47**, 2026 (1967).
(7) (a) J. A. Pople, J. W. McIver, Jr., and N. S. Ostlund, *J. Chem. Phys.*, **49**, 2965 (1968); (b) L. Salem and P. Loève, *ibid.*, **43**, 3402 (1965).
(8) G. Binsch, J. B. Lambert, B. W. Roberts, and J. D. Roberts, *J. Am. Chem. Soc.*, **86**, 5564 (1964); A. J. R. Bourn and E. W. Randall, *Mol. Phys.*, **8**, 567 (1964).
(9) A. Rauk, J. D. Andose, W. G. Frick, R. Tang, and K. Mislow, *J. Am. Chem. Soc.*, **93**, 6507 (1971).
(10) P. E. Stevenson and D. L. Burkey, *J. Am. Chem. Soc.*, **96**, 3061 (1974).
(11) J. W. Moskowitz and M. C. Harrison, *J. Chem. Phys.*, **43**, 3550 (1965).
(12) R. E. Kari and I. G. Csizmadia, *J. Chem. Phys.*, **56**, 4337 (1972).
(13) The data of Table III, ref 12, are fit to a third degree polynomial in the out-of-plane angle.
(14) G. Herzberg, "Infrared and Raman Spectra", Van Nostrand, Toronto, 1945.
(15) J. D. Swalen and J. A. Ibers, *J. Chem. Phys.*, **36**, 1914 (1962).
(16) Calculations employ computer programs CNINDO, by P. A. Dobosh, Quantum Chemistry Program Exchange (Indiana University), Program 141, which was modified for use in this study, and ATCOOR, by J. E. Nordlander.
(17) Reference 7a, Table II.
(18) (a) R. Wasylishen and T. Schaffer, *Can. J. Chem.*, **50**, 2989 (1972); (b) *ibid.*, **51**, 3087 (1973).
(19) Reference 9, p 6508.
(20) (a) M. Hollander and D. A. Wolfe, "Nonparametric Statistical Methods", Wiley, New York, 1973; (b) W. H. Kruskal and W. A. Wallis, *J. Am. Stat. Assoc.*, **47**, 583 (1952); (c) O. J. Dunn, *Technometrics*, **6**, 241 (1964).
(21) M. S. Gordon and H. Fischer, *J. Am. Chem. Soc.*, **90**, 2471 (1968); ref 9 and 10.

# The Electronic Structure of Pyrazine. A Valence Bond Model for Lone Pair Interactions

**Willard R. Wadt[1] and William A. Goddard III***

*Contribution No. 4970 from the Arthur Amos Noyes Laboratory of Chemical Physics, California Institute of Technology, Pasadena, California 91109.*
*Received September 23, 1974*

**Abstract:** A valence bond (VB) model is developed to describe the interaction of the lone pair excitations in pyrazine. Extensive ab initio minimal basis set (MBS) configuration interaction (CI) calculations show that the description of the n cations and $n\pi^*$ states of pyrazine afforded by the VB model is more accurate than that afforded by the molecular orbital (MO) model proffered by Hoffmann. The VB picture of the n cations and $n\pi^*$ states involves the interaction (resonance) of two *equivalent, localized* excitations. The resultant splitting is large (1 to 2 eV) because of a slight delocalization of the n orbitals induced by the Pauli principle. (The n orbitals remain 90% localized on the nitrogens.) The splitting of the $n\pi^*$ states is comparable to that of the n cations because the $\pi^*$ orbital is delocalized, even though the excitation process is localized on one nitrogen. The MBS CI calculations indicate that the lowest ionization potential of pyrazine corresponds to the $^2A_g(n)$ state. Calculations on the lowest Rydberg states indicate that they involve excitations out of an n orbital rather than a $\pi$ orbital, in opposition to earlier spectroscopic assignments. Finally, the calculations show that the forbidden $1^1B_{2g}(n\pi^*)$ state is 1 eV higher than the allowed $1^1B_{3u}(n\pi^*)$ state, so that the perturbations observed in the absorption spectrum must be ascribed to another source.

## I. Introduction

The nature of the excited states of pyrazine has generated great interest among spectroscopists and theoreticians for many years.[2] In addition to the $\pi \rightarrow \pi^*$ transitions, analogous to those of benzene, one expects new $n \rightarrow \pi^*$ transitions involving the nonbonding (or lone pair) orbitals on the nitrogen. Since there are two nitrogens in pyrazine, the question arises as to how the states involving excitations from the two different nitrogens interact with one another. With the advent of photoelectron spectroscopy,[3] the question has been extended to the interaction of the two possible n cations.

Two models for the interaction of the lone pairs have been previously developed, namely, the exciton model of El-Sayed and Robinson[4] and the molecular orbital (MO) model of Hoffmann.[5] The MO model has had good success in elucidating the photoelectron spectra (vide infra). In this paper we present an alternative model based on valence bond (VB) ideas. Ab initio minimal basis set (MBS) calculations have been carried out to test the usefulness of the VB model. In these calculations, emphasis has been placed on describing the $n\pi^*$ excited states and the n cations.

## II. Qualitative VB Model

**(A) n Cations.** To begin with, the VB view of the lone pairs in the ground state of pyrazine is represented by **1a**

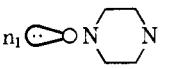


**1a**

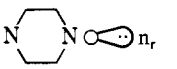


**1b**

and **1b**.[6] The nonbonding orbitals are represented by

and the electrons by dots. In the VB model the lone pairs ($n_l$ and $n_r$) are localized and equivalent, so that the ground state wave function is

$$\Psi = \mathcal{A}(\Phi_{core} n_l^2 n_r^2 \alpha\beta \ldots \alpha\beta)$$

where $\Phi_{core}$ represents the remaining electrons.

Now consider ionization of one of the lone pair electrons. One can remove the electron from either the left or right lone pair. These equivalent ion states are combined (resonance) to form two n cation states, $^2A_g$ and $^2B_{1u}$

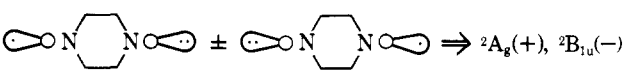


**2**

The wave functions in this approximation are[7]

$$\Psi(^2A_g) = (\Psi_L + \Psi_R)/\sqrt{2(1+S)} \quad (1)$$

$$\Psi(^2B_{1u}) = (\Psi_L - \Psi_R)/\sqrt{2(1-S)} \quad (2)$$

where[8]

$$\Psi_L = \mathcal{A}[(\Phi_{core})n_r^2 n_l \alpha\beta \ldots \alpha\beta\alpha] \quad (3)$$

$$\Psi_R = \mathcal{A}[(\Phi_{core})n_l^2 n_r \alpha\beta \ldots \alpha\beta\alpha] \quad (4)$$

and[9]

$$S = \langle \Psi_L | \Psi_R \rangle = -\langle n_l | n_r \rangle \quad (5)$$

The energy separation between these n-cation states is given by

$$\Delta E = E(^2A_g) - E(^2B_{1u})$$
$$= \frac{1}{2(1+S)}\langle \Psi_L + \Psi_R | \mathcal{H} | \Psi_L + \Psi_R \rangle - \frac{1}{2(1-S)}\langle \Psi_L - \Psi_R | \mathcal{H} | \Psi_L - \Psi_R \rangle$$

By symmetry $\langle \Psi_L | \mathcal{H} | \Psi_L \rangle = \langle \Psi_R | \mathcal{H} | \Psi_R \rangle$ and $\langle \Psi_L | \mathcal{H} | \Psi_R \rangle = \langle \Psi_R | \mathcal{H} | \Psi_L \rangle$ so that we obtain

$$\Delta E = \left(\frac{1}{1+S} - \frac{1}{1-S}\right)\langle \Psi_L | \mathcal{H} | \Psi_L \rangle + \left(\frac{1}{1+S} + \frac{1}{1-S}\right)\langle \Psi_L | \mathcal{H} | \Psi_R \rangle$$
$$= \frac{-2S}{1-S^2}\langle \Psi_L | \mathcal{H} | \Psi_L \rangle + \frac{2}{1-S^2}\langle \Psi_L | \mathcal{H} | \Psi_R \rangle$$
$$\Delta E = 2\langle \Psi_L | \mathcal{H} | \Psi_R \rangle - 2S\langle \Psi_L | \mathcal{H} | \Psi_L \rangle + \mathcal{O}(S^2) \quad (6)$$

Since $\Phi_{core}$ is taken to be the same in $\Psi_L$ and $\Psi_R$,[7] we need only consider the nonbonding orbitals $n_l$ and $n_r$ in evaluating (6). Moreover, the one-electron terms dominate the two-electron terms[10] so that (6) becomes [using $S = -S_{lr}$ from (5)]

$$\Delta E \cong 2\langle \Psi_L | h | \Psi_R \rangle + 2S_{lr}\langle \Psi_L | h | \Psi_L \rangle$$
$$= 2[-S_{lr}(h_{ll} + h_{rr}) - h_{lr}] + 2S_{lr}(2h_{rr} + h_{ll})$$
$$\Delta E = 2(S_{lr}h_{rr} - h_{lr}) \quad (7)$$

where

$$S_{lr} = \langle n_l | n_r \rangle$$
$$h_{lr} = \langle n_l | h | n_r \rangle$$
$$h_{ll} = \langle n_l | h | n_l \rangle$$
$$h_{rr} = \langle n_r | h | n_r \rangle.$$

Equation 7 has the same form as the one-electron exchange energy for the $H_2$ molecule, which is dominated by $S_{lr}t_{rr}$, where $t$ represents the kinetic energy operator.[11] Since $t_{rr}$ is positive

$$\Delta E \propto S_{lr} \quad (8)$$

Thus, we arrive at the very simple and intuitively reasonable result that the splitting energy is proportional to the overlap of the nonbonding orbitals.

Since the nitrogens are well separated (2.79 Å), one would expect the overlap of the atomic hybrid nonbonding orbitals to be quite small and positive; hence, considering only the n orbitals one would expect $\Delta E$ to be quite small and positive (that is, $^2B_{1u}$ lower). However, the effects on the atomic n orbitals of the other $\sigma$ and $\pi$ electrons present in pyrazine must be taken into account. Toward this end, we solve for the optimal wave functions [designated generalized valence bond (GVB)] of the form given in (1) and (2). Some rehybridization and scaling of n orbitals is expected, but the most important effect is induced by the Pauli principle.

Because of the Pauli principle, no more than two electrons can be symmetrically coupled or "paired up". As a result, electrons become partitioned into singlet (symmetric) pairs, e.g., CC, CH, and CN $\sigma$ bonds, $\pi$ bonds, 1s pairs, and lone pairs. The interaction between the singlet-coupled pairs is repulsive, so that the orbitals in different pairs tend to become orthogonal to one another. In the case of the nonbonding orbitals (singly or doubly occupied) nodal planes are expected to develop as shown in **3** in order to make the n orbital orthogonal (Pauli principle) to the $\sigma_{CC}$ and $\sigma_{CN}$ bonding pairs. Note that the nodal patterns of the n orbitals

**3**

favor a negative overlap. Thus, the effect of the Pauli-induced orthogonalization is to decrease $S_{lr}$ (algebraically) and it could make $S_{lr}$ negative. In fact, we find that the overlap is 0.0156 prior to orthogonalization and −0.106 after orthogonalization. Using (8), the Pauli orthogonalization reverses the predicted state ordering, leading to the $^2A_g$ state below the $^2B_{1u}$.

**(B) nπ* States.** Now we turn to the nπ* states. In **4** we show the ground state of pyrazine again except that the $\pi$ electrons are included (represented by circles, indicating 2p orbitals perpendicular to the plane of the paper) and are shown coupled into the two VB Kekulé structures. The tie

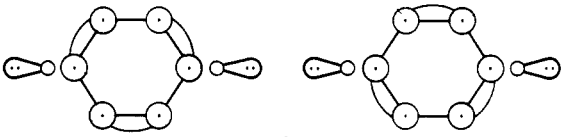

**4**

lines indicate a pair of orbitals singlet coupled into a $\pi$ bond. The simplest VB model for the n → π* excitation involves promotion of an electron from a nonbonding orbital to the $p_\pi$ orbital on the same nitrogen. In this manner electroneutrality of all the atoms is maintained. There are three ways to pair the $\pi$ orbitals into bonds in this case. Note that

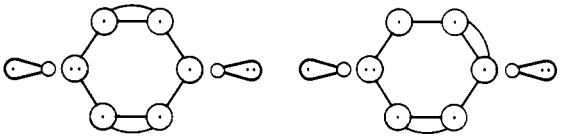

**5a** **5b**

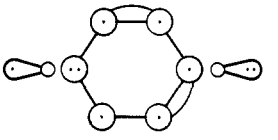

**5c**

although the electron promotion (n → π) is assumed to be localized on one nitrogen, the resulting unpaired $\pi$ orbital is on either the ortho carbons or on the para nitrogen.

Exciting a lone pair electron from the right nitrogen leads to a comparable set of nπ* configurations which must be combined (resonance) with those in **5** to get states of the correct total symmetry. Using the same arguments as be-

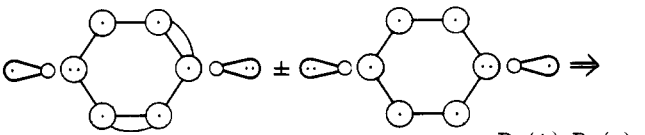

$B_{3u}(+)$, $B_{2g}(-)$

**6**

fore, the splitting of the nπ* states is expected to be propor-

tional to the product of the lone pair and $\pi^*$ orbital overlaps.

$$\Delta E = E(B_{3u}) - E(B_{2g}) \propto S_{n_l n_r} S_{\pi_l^* \pi_r^*} \quad (9)$$

The $\pi^*$ orbitals are quite delocalized, so that the splitting energy of the $n\pi^*$ states is expected to be only slightly smaller than that of the n cations.

Determining the sign of $S_{\pi_l^* \pi_r^*}$ and, hence, $\Delta E$ requires examination of the three couplings of the $\pi$ orbitals. In **7** we show the approximate position of the nodal planes that will be induced by the Pauli principle to make the $\pi^*$ orbital orthogonal to three pairs of $\pi$ electrons. (The $\sigma$ structure is suppressed). Making the phases of the three structures consistent, we see that the $\pi^*$ orbital will have the form

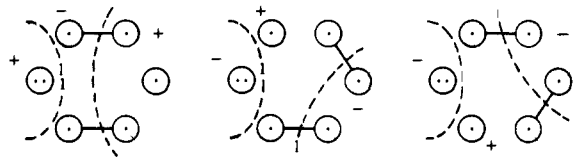

**7a** **7b** **7c**

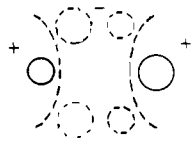

**8**

so that the overlap, $S_{\pi_l^* \pi_r^*}$, will be positive and

$$\Delta E = E(B_{3u}) - E(B_{2g}) < 0$$

or

$$E(B_{3u}) < E(B_{2g})$$

The $B_{3u}$ $n\pi^*$ states are stabilized with respect to the $B_{2g}$.

Finally, unpaired n and $\pi^*$ orbitals may be singlet or triplet coupled, giving rise to $^1n\pi^*$ and $^3n\pi^*$ states. The energies of these are given by

$$E(^1n\pi^*) = E_0 + K$$

$$E(^3n\pi^*) = E_0 - K$$

where $K = \langle n\pi^* | n\pi^* \rangle$ is the two-electron exchange integral between the unpaired n and $\pi^*$ orbitals. Since $K$ is positive, the triplet is lower than the singlet. We will later consider self-consistent adjustments of the VB orbitals (i.e., GVB). Since $-K$ is negative for the triplet state, we expect the orbitals for the triplet to readjust so as to increase $K$, while those for the singlet state should readjust so as to decrease $K$. Thus configurations **5b** and **5c** with the $\pi^*$ orbital on the ortho carbon are favored for the triplet, while **5c** with the $\pi^*$ orbital on the para nitrogen is favored for the singlet. In fact, to increase further the value of $K$ for the $^3n\pi^*$ state, the following ionic configurations are expected to come into play.

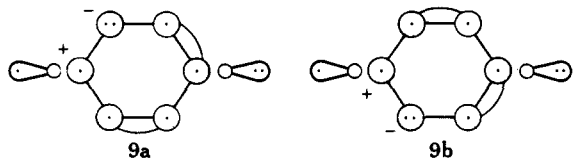

**9a** **9b**

## III. Qualitative MO Model

We present a brief description of the MO model for lone pair interaction developed by Hoffmann[5] in order to compare it with the VB model. To begin with, symmetry orbitals ($n_+$ and $n_-$) are formed from the localized (VB type) nonbonding orbitals, $n_l$ and $n_r$

$$n_+ = (n_l + n_r)/\sqrt{1 + S_{lr}}$$

$$n_- = (n_l - n_r)/\sqrt{1 - S_{lr}}$$

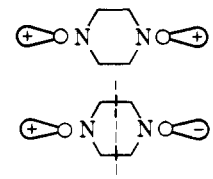

where $S_{lr} = \langle n_l | n_r \rangle$. The separation of the orbital energies, $\Delta\epsilon$, for $n_+$ and $n_-$ is

$$\Delta\epsilon = \epsilon(n_+) - \epsilon(n_-) = \langle n_+ | \mathcal{H} | n_+ \rangle - \langle n_- | \mathcal{H} | n_- \rangle = \frac{2}{1 - S_{lr}^2} \langle n_l | \mathcal{H} | n_r \rangle - \frac{2S_{lr}}{1 - S_{lr}^2} \langle n_l | \mathcal{H} | n_l \rangle$$

or by arguments similar to those used before

$$\Delta\epsilon \propto -S_{lr}$$

The splitting of the orbital energies is proportional to minus the overlap of the lone pairs. Since for localized n orbitals $S_{lr}$ is small and positive, we have

$$\Delta\epsilon = \epsilon(n_+) - \epsilon(n_-) < 0$$

or as expected

$$\epsilon(n_+) < \epsilon(n_-)$$

This corresponds to what Hoffmann[5] calls "through space" interaction.

Now, we must consider the effects of the other $\sigma$ and $\pi$ electrons by performing a simple Hartree-Fock (HF) calculation. Hoffmann[5] found that the key interactions are between the n orbitals and the $\sigma$ orbitals associated with the $\sigma_{CC}$ bonds. Since the interaction of two orbitals with different symmetry vanishes, the $n_+$ orbital interacts only with the $\sigma_{CC}$ orbitals, while the $n_-$ orbital interacts only with the $\sigma_{CC}^*$ orbitals. Simple perturbation arguments indicate that these interactions tend to stabilize $n_+$ with respect to $n_-$ as shown in the diagram below. Hoffmann[5] refers to the resultant splitting of $n_+$ and $n_-$ as "through bond" interaction.

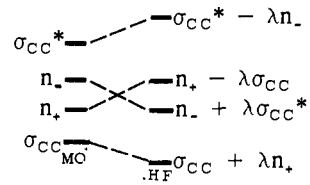


Using Koopmans' theorem[12] to equate the vertical ionization potential with the negative of the orbital energy, the "through bond" interaction leads to the following ordering of the n cations: $E(^2A_g) < E(^2B_{1u})$, i.e., an electron in the $n_+$ orbital is easier to ionize than one in the $n_-$ orbital. This result is in agreement with the conclusion of the VB model.

The MO model for the $n \rightarrow \pi^*$ excitations assumes that the lowest transitions will be to the lowest unoccupied $\pi^*$ MO, namely, the $2b_{3u}$ shown in **10**

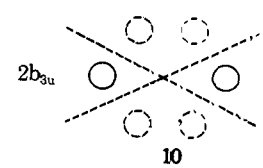


**10**

Therefore, the lowest $n\pi^*$ state is expected to arise from the excitation $n_+ \rightarrow 2b_{3u}$, giving the $B_{3u}(n\pi^*)$ state. The excitation $n_- \rightarrow 2b_{3u}$ leads to the $B_{2g}(n\pi^*)$ state at a higher energy, again in agreement with the VB model. The splitting of the $B_{3u}$ and $B_{2g}(n\pi^*)$ states is predicted to be comparable to that of the n cations.

## IV. Qualitative Comparison of the VB and MO Models

At one level the VB and MO models for lone pair interaction seem quite similar. Both begin by considering atomic-like lone pairs which have small overlap and, hence, a small splitting. Then the rest of the pyrazine molecule is taken into account. Upon optimization for the molecule, the orbitals delocalize, leading to large changes in the overlap and splitting energy. Moreover, the delocalization effects are such that the splitting energy changes sign relative to the small atomic lone pair interaction. Finally, the $\pi^*$ orbital is delocalized in both cases.

On the other hand, the methods by which the interactions are explained and evaluated are radically different. In the VB model the splitting energies arise from the interaction (resonance) of two many-electron wave functions (configurations) that describe two equivalent excitation processes. In the MO model the splittings arise from the interaction of *ground state* orbitals (one-electron wave functions). As a result, the ground state lone pair orbitals are localized and equivalent in VB but delocalized and inequivalent in MO. Furthermore, the excitation process giving rise to the n cations or $n\pi^*$ states is localized on one nitrogen in VB but delocalized over both nitrogens in MO.

We believe (vide infra) that the VB model provides a picture that is closer to the results of more exact wave functions than the MO model. Support for this contention may be found prior to any calculations. For example, in the VB model only the total wave function reflects the full symmetry of the molecule. The component configurations are allowed to have a lower symmetry ($C_{2v}$ instead of $D_{2h}$). This freedom allows the excitation to be localized on one nitrogen as well as allowing the remaining occupied orbitals to adjust or polarize in response to the excitation as was evident in the difference of the $\pi^*$ orbitals for the $^1n\pi^*$ and $^3n\pi^*$ states. On the other hand, in the MO (or HF) model the individual orbitals are *forced* to be symmetry functions, and hence delocalized.

Forcing the excited states to be described in terms of a one-electron promotion between two delocalized orbitals can lead to problems. For instance, consider the $n\pi^*$ states described by $n_+ \rightarrow \pi^*$ in the MO model. Recalling that the $\pi^*$ orbital ($2b_{3u}$) on the nitrogens is given roughly by $\pi_l + \pi_r$, we have

$$\begin{aligned} n_+\pi^* &= (n_l + n_r)(\pi_l + \pi_r) \\ &= \underbrace{(n_l\pi_l + n_r\pi_r)}_{\text{covalent}} + \underbrace{(n_l\pi_r + n_r\pi_l)}_{\text{ionic}} \end{aligned}$$

so that the wave function is forced to have comparable amounts of covalent and ionic character. The resulting excitation energies are much too high (vide infra).

The difficulties of using symmetry orbitals are not as apparent in the case of the n cations. Consider the MO wave function for the $^2A_g$ state

$$\begin{aligned} \Psi^{MO}(^2A_g) &= \mathcal{A}[(\Phi_{core})n_-^2n_+\alpha\beta\ldots\alpha\beta\alpha] \\ &= \mathcal{A}[(\Phi_{core})(n_l - n_r)^2(n_l + n_r)\alpha\beta\ldots\alpha\beta\alpha] \\ &= \mathcal{A}[(\Phi_{core})(n_l^2n_r + n_r^2n_l)\alpha\beta\ldots\alpha\beta\alpha] = \\ &\qquad (\Psi_L + \Psi_R)/\sqrt{1+S} \end{aligned}$$

which is equivalent to the simple VB wave function. However, when solving for the $^2A_g$ state variationally, $\Phi_{core}$ is forced to be symmetric in the HF wave function but is allowed to polarize differently for $\Psi_L$ and for $\Psi_R$ in the GVB wave function.

Finally, although the MO model for lone pair interaction is based on the ground state orbitals, these orbitals are not uniquely defined. One can apply an arbitrary unitary transformation to the space of occupied HF orbitals without changing the energy. This fact adds a note of uncertainty to the MO model. How are the orbitals produced by an HF calculation defined? The answer is Koopmans' theorem.[12]

Previously we mentioned that Koopmans' theorem allows one to equate vertical ionization potentials with the negative orbital energies. There is actually more to it. For an HF wave function the energy of the ground ($N$ electron) state may be related to the various cation ($N-1$ electron) state energies via the orbital energy, i.e.

$$E_{N-1} = E_N - \epsilon$$

However, since the orbitals and orbital energies are not uniquely defined by the HF calculation, one is faced with an infinity of choices for the cation energy. Koopmans[12] concluded that the best choice of $\epsilon$ would lead to the lowest energy for $E_{N-1}$. Consequently, the value of $\epsilon$ is maximized and the resulting orbital becomes well defined. Therefore, we see that the MO's for the ground state are actually defined so as to reflect the nature of the various cations. This explains how the two ground state lone pair orbitals, $n_+$ and $n_-$, are calculated to be inequivalent by HF. The inequivalence actually arises upon ionization or excitation from the n orbitals as shown in the VB model.

## V. Calculational Details

The goal of the calculations reported herein is to test some of the current concepts concerning the excited states of pyrazine, particularly those proffered in the VB model. To do this it is important to allow the orbitals to delocalize and readjust in the presence of other electrons. For example, the orbitals of the n cation (in $\Psi_L$ and $\Psi_R$) are expected to polarize in response to the n ionization as shown in **11**.

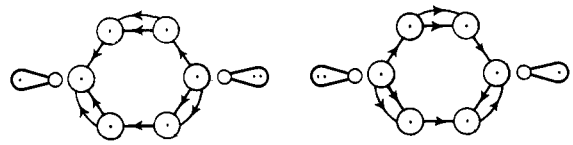

**11**

The method of calculating these effects is the generalized valence bond (GVB) method.[13] However, because the orbitals in $\Psi_L$ and $\Psi_R$ are, in general, nonorthogonal, evaluating expressions such as $\langle\Psi_L|\mathcal{H}|\Psi_R\rangle$ involves ~21! or 22! terms and is not currently feasible. Therefore, we designed a configuration interaction (CI) calculation that would mimic the GVB wave function.

**(A) Localized n Orbitals.** The brute force method would be to take the ground state ($^1A_g$) HF vectors and perform a large scale CI among the 28 valence orbitals. Because of the large number of orbitals, this procedure is cumbersome and the results are not easy to interpret in terms of simple concepts. The major problem with using HF ground state vectors is that the orbitals are *not* uniquely partitioned into orbitals of different character (lone pair, CC bonding, CH bonding, etc.) so that an extensive CI is required to ensure inclusion of all the important effects. In order to obtain unique nonbonding orbitals for the CI calculations, we performed open-shell HF calculations with a fully convergent SCF program[14] on the $^2n$, $^1n\pi$, and $^3n\pi$ states, allowing the symmetry to be reduced to $C_{2v}$. In other words, in each case we solved for one of the resonant configurations. The singly-occupied nonbonding orbital is uniquely defined in each of the three wave functions. As shown by the contour plots in Figure 1 and the Mulliken populations in Table I, the nonbonding orbital is in each case quite localized on one nitrogen (88–90%). Since all three nonbonding orbitals are so similar, we chose one, the $^3n\pi^*$ orbital, to partition the HF space into n and $\sigma$ orbitals.

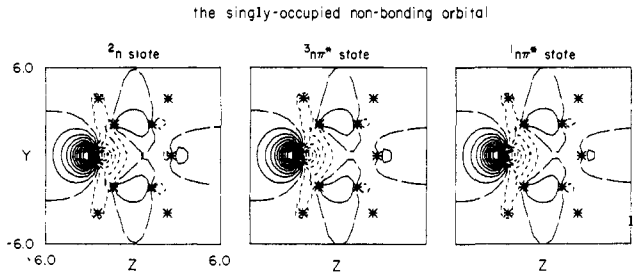


**Figure 1.** Contour plots of the singly-occupied n orbital from the $^2$n, $^3$nπ*, and $^1$nπ* SCF wave functions. The contour increment is 0.05 au.

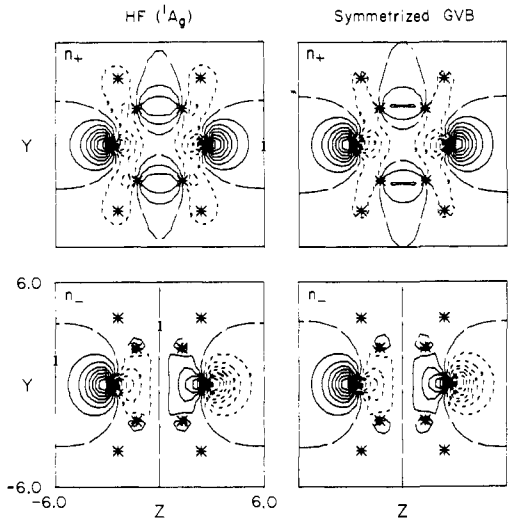


**Figure 2.** Contour plots of the HF $1^1A_g$ and symmetrized GVB $n_+$ and $n_-$ orbitals. The contour increment is 0.05 au.

Table I. Mulliken Populations for the Singly-Occupied n Orbital

| | | $^2$n | $^1$nπ* | $^3$nπ* |
|---|---|---|---|---|
| Excited N | s | 0.163 | 0.155 | 0.172 |
| | z | 0.719 | 0.735 | 0.722 |
| | Total | 0.882 | 0.890 | 0.894 |
| Ortho C | | 0.037 | 0.036 | 0.035 |
| Ortho H | | 0.020 | 0.019 | 0.019 |
| Meta H | | 0.008 | 0.008 | 0.007 |
| Para N | | 0.011 | 0.006 | 0.009 |

Table II. Mulliken Populations for the n Symmetry Orbitals from the $^1A_g$, $^2A_g$, and $^2B_{1u}$ States

| | | | $n_+$ | | $n_-$ | |
|---|---|---|---|---|---|---|
| | | | GVB | HF | GVB | HF |
| $^1A_g$ | N | s | 0.171 | 0.120 | 0.185 | 0.176 |
| | | z | 0.678 | 0.566 | 0.760 | 0.759 |
| | | Total | 0.849 | 0.686 | 0.945 | 0.935 |
| | C | | 0.098 | 0.216 | 0.049 | 0.054 |
| | H | | 0.053 | 0.097 | 0.006 | 0.010 |
| $^2A_g$ | N | s | 0.166 | 0.129 | 0.188 | 0.181 |
| | | z | 0.696 | 0.628 | 0.749 | 0.738 |
| | | Total | 0.862 | 0.757 | 0.937 | 0.919 |
| | C | | 0.097 | 0.179 | 0.058 | 0.067 |
| | H | | 0.041 | 0.063 | 0.005 | 0.014 |
| $^2B_{1u}$ | N | s | 0.175 | 0.133 | 0.186 | 0.180 |
| | | z | 0.675 | 0.588 | 0.768 | 0.773 |
| | | Total | 0.850 | 0.721 | 0.954 | 0.953 |
| | C | | 0.102 | 0.195 | 0.041 | 0.043 |
| | H | | 0.047 | 0.083 | 0.005 | 0.004 |

Table III. H-Atom Mulliken Populations for the $\sigma_{CH}$ Orbitals

| State | $\sigma_{CH}$ | Total Hσ | $\sigma_{CH}$* | Total Hσ* |
|---|---|---|---|---|
| $^1A_g$ | 0.684 | 0.732 | 1.152 | 1.268 |
| $^2A_g$ | 0.594 | 0.645 | 1.169 | 1.355 |
| $^2B_{1u}$ | 0.608 | 0.653 | 1.164 | 1.347 |

Starting with the localized n orbital, symmetry functions ($n_+$ and $n_-$) were formed and projected onto the space of the occupied HF orbitals for the $^1A_g$, $^2A_g$, and $^2B_{1u}$ states[15] to obtain localized $n_+$ and $n_-$ orbitals for each state. The remaining occupied σ orbitals for each state were orthogonalized to the new n orbitals. In this manner, we partitioned the HF occupied space into n and σ orbitals, greatly facilitating the CI calculations. The fact that the simple HF calculation on the ground state mixes extra σ character into the n orbitals (especially $n_+$) is shown in Figure 2 and Table II, where contour plots and Mulliken populations are presented for the HF and the symmetrized GVB n orbitals, respectively. Note how the $n_-$ orbital is naturally more localized than the $n_+$ because of the node through the CC bond.

Before describing the CI calculations, we should state that SCF calculations were performed using Huzinaga's[16] (7s, 3p/3s) set of primitive Gaussian basis fuctions contracted to a MBS [2s, 1p/1s] by Dunning.[17] All calculations were carried out at the experimental equilibrium geometry for pyrazine.[2]

(B) **n-π CI.** In all the CI calculations, the self-consistent $^2A_g$ and $^2B_{1u}$ vectors were used for the respective n cations, while the $^1A_g$ vectors were employed for all the states of the neutral species as well as for the π cations. Eight different types of CI calculations were performed:

(1) HF CI, only the HF configuration was included; (2) S CI, the HF configuration plus single excitations into the π space (six orbitals); (3) π CI, the HF configuration plus a full CI within the π space (six orbitals); (4) n-π CI, the HF configuration plus a full CI within the n + π space (eight orbitals).

(C) **Relaxation of the σ Core.** In the above four CI calculations the same doubly-occupied σ orbitals are used for all states. In order to test the importance of the polarization of the CN, CC, and CH bonds, two more CI calculations were designed. It was not feasible to include the entire valence σ space (20 orbitals) along with the 2 n and 6 π orbitals.[18] Therefore, we partitioned the σ space into the 12 $\sigma_{CC}$ and $\sigma_{CN}$ orbitals and the 8 $\sigma_{CH}$ orbitals. This partition has the added advantage that the $\sigma_{CC}$ and especially the $\sigma_{CN}$ orbitals are expected to polarize more than the $\sigma_{CH}$ orbitals in the n cations and nπ* states.

The σ orbitals were partitioned by taking the two σ or σ* orbitals for each symmetry type that had the greatest CH character and combining them in such a way that the p function on the carbon was directed toward the hydrogen. The success of this simple partitioning is shown in Table III where the H atom Mulliken populations in the $\sigma_{CH}$ and $\sigma^*_{CH}$ orbitals are compared with the total H populations. We see that the $\sigma_{CH}$ orbitals constructed in this manner account for about 90% of the total CH space.

The two CI's allowing relaxation in the σ orbitals are denoted as (5) $\sigma_{CC/CN}$ POL(1) CI and (6) $\sigma_{CH}$ POL(1) CI. Both CI's include all the configurations in the n-π CI plus single excitations in the $\sigma_{CC}/\sigma_{CN}$ or $\sigma_{CH}$ space from two basic configurations. One of the two basic configurations is the HF configuration, while the other allows the lone pair excitation to localize on one nitrogen. For example, the HF configuration of the $^2A_g$ state is

$$\mathcal{A}[(\Phi_{core})n_-^2n_+\alpha\beta,\ldots\alpha\beta\alpha]$$

while the second basic configuration is

$$\mathcal{A}[(\Phi_{core})n_+^2n_-\alpha\beta,\ldots\alpha\beta\alpha]$$

Taking + and − combinations of the above configurations gives

$$\mathcal{A}[(\Phi_{core})n_l^2 n_r \alpha\beta \ldots \alpha\beta\alpha]$$

and

$$\mathcal{A}[(\Phi_{core})n_r^2 n_l \alpha\beta \ldots \alpha\beta\alpha]$$

so that inclusion of both configurations allows relaxation of the $\sigma$ orbitals in response to the localized excitation.

**(D) Further Relaxation of the $\pi$ Space.** A final set of CI calculations was performed using a slightly extended basis. The MBS was augmented by the most diffuse $p_x$ primitive in Huzinaga's[16] (3p) set. This basis set is designated MBS + DZ($\pi$). Two CI calculations were performed allowing relaxation of the $\pi$ orbitals with the added six "double $\zeta$" $\pi$ virtuals: (7) $\pi$ POL(2) CI and, (8) $\pi$ POL(3) CI. In the $\pi$ POL(2) CI all the configurations in the n-$\pi$ CI were included plus all those arising from single and double excitations from the ground state HF configuration [within a 14 (2n + 12$\pi$) orbital space] with the restriction that only single excitations are allowed into the "double $\zeta$" $\pi$ space. The $\pi$ POL(3) CI is the same as the $\pi$ POL(2) CI except that up to triple excitations are allowed from the ground HF configuration.

**(E) Rydberg States.** Simple calculations were also made to locate the position of the lowest singlet Rydberg states arising from excitations out of the two most loosely bound orbitals $6a_g(n_+)$ and $1b_{1g}(\pi)$. In order to describe the diffuse Rydberg states two augmented basis sets were employed.

(9) MBS + R($\sigma$): MBS augmented with two diffuse s, $p_y$, and $p_z$ functions centered at the CC bond midpoints and at the nitrogens. The carbon exponents were 0.060 and 0.020, while the nitrogen exponents were 0.075 and 0.025.

(10) MBS + R($\pi$): MBS augmented with two diffuse $p_x$ functions centered at each of the four carbons and two nitrogens. The exponents were the same as for MBS + R($\sigma$).

The Rydberg states were calculated using the improved virtual orbital (IVO) method.[19] In this method the SCF occupied orbitals from the ground state (or excited state) are used and the correct excited state hamiltonian for the virtual orbitals (without self-terms) is solved, yielding a whole spectrum of excited states from one calculation. IVO calculations on $H_2O$[19,20] and $O_2$[21] have led to good agreement with experiment. In general, the calculations on pyrazine used ground state orbitals, although a few runs were made with the appropriate cation orbitals.

## VI. Results

**Ramifications for the VB Model. (A) n Cations.** The various SCF and CI results for the n cations are listed in Table IV. First we see that in every case the $^2A_g$ state is lower than the $^2B_{1u}$ state as predicted by both the VB and MO models. However, even the simple SCF results point to important differences in the two models. When the lone pair ionization is allowed to localize on one nitrogen as in the VB model, the energy drops significantly (0.8 eV relative to the $^2A_g$ state). Therefore, we may conclude that the description of the n cations in terms of resonant and antiresonant combinations of localized excitations (VB) is more correct than the description in terms of interactions of symmetry orbitals (MO).

Correlating the $\pi$ system ($\pi$ CI) lowers the absolute energies of the $^2A_g$ and $^2B_{1u}$ states by 2.4 eV, but the ionization potentials are unchanged. That is, the $\pi$ correlation energies of the ground state and n cations are comparable. In this $\pi$ CI, the ionization is still forced to arise from a delocalized symmetry orbital. On the other hand, as soon as the CI calculation includes configurations that allow a localized description of the excitation, as in the n-$\pi$ CI, the energies of the n cations drop dramatically relative to the ground state.[22] The excitation energy to the $^2A_g$ state drops 1.2 eV, while that to the $^2B_{1u}$ state drops 1.6 eV.

Table IV. SCF and CI Results for the n Cations (in eV)

| | Vertical ionization potentials | | Splitting energies | CI energy lowerings | |
|---|---|---|---|---|---|
| | $^2A_g$ | $^2B_{1u}$ | $\Delta E$ | $^2A_g$ | $^2B_{1u}$ |
| **Nonlocalized Wave Functions** | | | | | |
| MO level | | | | | |
| Koopmans' theorem | 12.03 | 14.70 | 2.67 | −0.71 | −1.15 |
| SCF | 11.32 | 13.55 | 2.23 | 0.0 | 0.0 |
| S CI | 11.51 | 13.37 | 1.86 | −0.40 | −0.02 |
| CI level | | | | | |
| $\pi$ CI | 11.48 | 13.36 | 1.88 | 2.04 | 2.39 |
| **Localized Wave Functions** | | | | | |
| MO level | | | | | |
| SCF | 10.52 | | | | |
| CI level—no $\sigma$ readjustment | | | | | |
| n-$\pi$ CI | 10.27 | 11.70 | 1.43 | 3.32 | 4.12 |
| $\pi$ POL(2) CI | 10.01 | 11.51 | 1.48 | 3.92 | 4.66 |
| CI level—$\sigma$ readjustment | | | | | |
| $\sigma_{CH}$POL(1) CI | 10.24 | 11.72 | 1.48 | 3.42 | 4.17 |
| $\sigma_{CC/CN}$POL(1) CI | 9.81 | 11.45 | 1.64 | 3.88 | 4.48 |
| POL CI[a] | 9.52 | 11.28 | 1.76 | 4.58 | 5.07 |
| Experiment[b] | 9.63 | 11.35 | 1.72 | | |

[a] POL CI: energy lowerings for the three POL CI's (each with respect to the n-$\pi$ CI) are combined assuming pairwise additivity. [b] Reference 25.

Analysis of the CI wave functions reinforces the VB model of localized excitations. For example, after the HF configuration (CI coefficient = 0.90) the most important configuration (CI coefficient = 0.25) in the n-$\pi$ CI wave function for the $^2A_g$ state is a double excitation with respect to the HF configuration, namely $5b_{1u}(n_-) \rightarrow 6a_g(n_+)$, $1b_{2g}(\pi) \rightarrow 2b_{3u}(\pi^*)$. The effect of this configuration may be revealed by considering just the four orbitals $5b_{1u}(n_-)$, $6a_g(n_+)$, $1b_{2g}(\pi)$, and $2b_{3u}(\pi^*)$ represented by $(n_l - n_r)$, $(n_l + n_r)$, $(\pi_l - \pi_r)$ and $(\pi_l + \pi_r)$, respectively. Then, the HF configuration is

$$n_-^2 n_+ \pi^2 = (n_l - n_r)^2 (n_l + n_r)(\pi_l - \pi_r)^2 = (n_l^2 n_r + n_r^2 n_l)(\pi_l^2 - \pi_l\pi_r - \pi_r\pi_l + \pi_r^2)$$

and the second dominant configuration is[23]

$$n_+^2 n_- (\pi\pi^* + \pi^*\pi) = (n_l + n_r)^2 (n_l - n_r)[(\pi_l - \pi_r)(\pi_l' + \pi_r) + (\pi_l + \pi_r)(\pi_l - \pi_r)] = (n_r^2 n_l - n_l^2 n_r)(\pi_l^2 - \pi_r^2)$$

Adding these two configurations leads to configurations of the form

$$n_r^2 n_l \pi_l^2$$

$$n_l^2 n_r \pi_r^2$$

which clearly represent the polarization of the $\pi$ system toward the ionized nitrogen.

Since polarization of the $\pi$ system is important in the n cations, one would expect polarization of the $\sigma$ system to be significant. We found that relaxation of the $\sigma_{CC}$ and $\sigma_{CN}$ orbitals lowers the energy by 0.4–0.5 eV, while relaxation of the $\sigma_{CH}$ orbitals lowers the energy by 0.05–0.1 eV. These results are in accord with our conjecture that the CH bonds (further removed from the excited nitrogen) polarize much less than the $\sigma_{CN}$ bonds adjacent to the excited nitrogen.

Finally, the fact that the $\pi$ POL(2) CI leads to an absolute energy lowering of ~0.6 eV and a decrease in the ion-

Table V. SCF and CI Results for the $^3n\pi^*$ States (in eV)

| | Vertical excitation energies | | Splitting energies | CI energy lowerings | |
|---|---|---|---|---|---|
| | $^3B_{3u}$ | $^3B_{2g}$ | $\Delta E$ | $^3B_{3u}$ | $^3B_{2g}$ |
| Nonlocalized Wave Functions | | | | | |
| MO level | | | | | |
| S CI | 3.97 | 5.71 | 1.74 | 0.0 | 0.0 |
| CI level | | | | | |
| $\pi$ CI | 4.95 | 6.72 | 1.77 | 1.44 | 1.41 |
| Localized Wave Functions | | | | | |
| MO level | | | | | |
| SCF | 3.41 | | | | |
| CI level—no $\sigma$ readjustment | | | | | |
| n–$\pi$ CI | 3.39 | 4.53 | 1.14 | 3.06 | 3.66 |
| $\pi$ POL(2) CI | 3.07 | 4.32 | 1.25 | 3.72 | 4.22 |
| CI level—$\sigma$ readjustment | | | | | |
| $\sigma_{CH}$POL(1) CI | 3.37 | 4.53 | 1.16 | 3.15 | 3.73 |
| $\sigma_{CC/CN}$POL(1) CI | 2.94 | 4.31 | 1.37 | 3.52 | 4.05 |
| POL CI[a] | 2.60 | 4.03 | 1.43 | 4.26 | 4.68 |
| Experiment[b] | 3.2–3.3 | | | | |

[a] POL CI: energy lowerings for the three POL CI's (each with respect to the n–$\pi$ CI) are combined assuming pairwise additivity. [b] Reference 2.

Table VI. SCF and CI Results for the $^1n\pi^*$ States (in eV)

| | Vertical excitation energies | | Splitting energies | CI energy lowerings | |
|---|---|---|---|---|---|
| | $^1B_{3u}$ | $^1B_{2g}$ | $\Delta E$ | $^1B_{3u}$ | $^1B_{2g}$ |
| Nonlocalized Wave Functions | | | | | |
| MO level | | | | | |
| S CI | 5.17 | 7.04 | 1.87 | 0.0 | 0.0 |
| CI level | | | | | |
| $\pi$ CI | 6.12 | 8.00 | 1.88 | 1.45 | 1.45 |
| Localized Wave Functions | | | | | |
| MO level | | | | | |
| SCF | 4.09 | | | | |
| CI level—no $\sigma$ readjustment | | | | | |
| n–$\pi$ CI | 4.19 | 5.25 | 1.06 | 3.46 | 4.27 |
| $\pi$ POL(2) CI | 3.90 | 5.08 | 1.18 | 4.09 | 4.78 |
| CI level—$\sigma$ readjustment | | | | | |
| $\sigma_{CH}$POL(1) CI | 4.17 | 5.26 | 1.09 | 3.55 | 4.33 |
| $\sigma_{CC/CN}$POL(1) CI | 3.75 | 5.05 | 1.30 | 3.89 | 4.63 |
| POL CI[a] | 3.44 | 4.89 | 1.45 | 4.61 | 5.20 |
| Experiment[b] | 3.8–3.9 | | | | |

[a] POL CI: energy lowerings for the three POL CI's (each with respect to the n–$\pi$ CI) are combined assuming pairwise additivity. [b] Reference 2.

ization potentials of ~0.2 eV indicates that the atomic scaling of the $p_x(\pi)$ orbitals is not appropriate for either the ground state or n cations. Similar results may hold true for the $\sigma$ system, indicating a need to perform double $\zeta$ calculations.

Since the configurations added to the n–$\pi$ CI in the three POL CI's are mutually exclusive (exactly in a mathematical sense and roughly in a physical sense), one can sum the respective CI lowerings to get a reasonable estimate of the CI energies to be obtained if the POL CI's are carried out simultaneously. The vertical ionization potentials for the $^2A_g$ and $^2B_{1u}$ states are predicted at 9.53 and 11.27 eV. Comparison with photoelectron spectra will be made later in this section.

(B) $n\pi^*$ **States.** The various SCF and CI results for $^3n\pi^*$ and $^1n\pi^*$ states are listed in Table V and Table VI, respectively. Just as for the n cations, HF calculations enforcing $D_{2h}$ symmetry lead to much larger excitation energies than when the orbitals are allowed to localize (the S CI results of Tables V and VI are essentially equivalent to those of self-consistent HF calculations using symmetry orbitals). Thus, the VB model of localized excitations is more appropriate than the delocalized model.

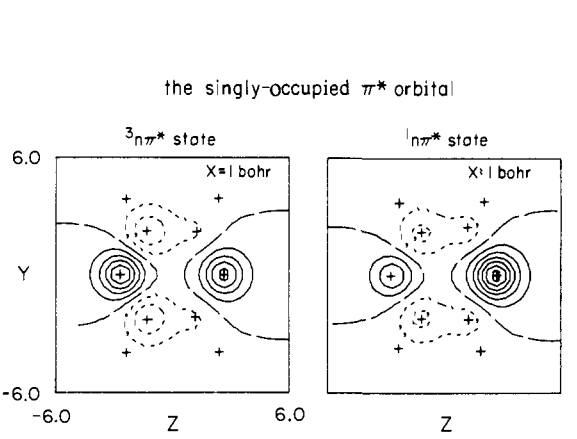


**Figure 3.** Contour plots of the singly occupied $\pi^*$ orbital from the $^3n\pi^*$ and $^1n\pi^*$ SCF wave functions. The contour increment is 0.05 au.

As discussed previously, using $D_{2h}$ symmetry orbitals not only forces the excitation to be delocalized, but introduces significant ionic character into the wave function. Neither of these effects are removed by correlating the $\pi$ system. In fact, with the $\pi$ CI the excitation energies to the $n\pi^*$ states increase by 1 eV since there is 1 eV more correlation in the ground state six-electron $\pi$ system than in the seven-electron $\pi$ system of the $n\pi^*$ states.[24]

The CI results for the $n\pi^*$ states are very similar to those for the n cation. Allowing the excitation to localize as in the n–$\pi$ CI decreases the $n\pi^*$ excitation energies by 1.5 to 2.8 eV! The splitting energies are also reduced by 0.8 eV. The most important configurations apart from the HF configuration are the double excitations $n_+ \rightarrow n_-$, $\pi \rightarrow \pi^*$ or $n_- \rightarrow n_+$, $\pi \rightarrow \pi^*$ that allow the excitation to localize. For example, in the $^1B_{3u}$ state the HF configuration has a coefficient of 0.87, while the next most important configuration arises from the double excitation $5b_{1u}(n_-) \rightarrow 6a_g(n_+)$, $1b_{2g}(\pi) \rightarrow 2b_{3u}(\pi^*)$ with coefficient 0.31. In this case the HF configuration is

$$n_-^2 n_+ \pi^2 \pi^* = (n_l - n_r)^2 (n_l + n_r)(\pi_l - \pi_r)^2 (\pi_l + \pi_r) = (n_l^2 n_r + n_r^2 n_l)(\pi_l^2 \pi_r - \pi_r \pi_l^2 + \pi_r^2 \pi_l - \pi_l \pi_r^2)$$

and the second configuration

$$n_+^2 n_- \pi \pi^{*2} = (n_l + n_r)^2 (n_l - n_r)(\pi_l - \pi_r)(\pi_l + \pi_r)^2 = (n_r^2 n_l - n_l^2 n_r)(\pi_l^2 \pi_r - \pi_r \pi_l^2 - \pi_r^2 \pi_l + \pi_l \pi_r^2)$$

Adding these two leads to

$$n_l^2 n_r (\pi_r^2 \pi_l - \pi_l \pi_r^2) + n_r^2 n_l (\pi_l^2 \pi_r - \pi_r \pi_l^2)$$

or

$$n_l^2 n_r \pi_r (\pi_r \pi_l + \pi_l \pi_r) + n_r^2 n_l \pi_l (\pi_l \pi_r + \pi_r \pi_l)$$

the appropriate localized excitation.

As in the case of the n cation, relaxation of the $\sigma_{CN}$ and $\sigma_{CC}$ orbitals is much more important than relaxing the $\sigma_{CH}$ orbitals. Again, the $\pi$ POL(2) CI indicates that double $\zeta$ calculations are warranted to optimize the scale of the orbitals. The POL CI's tend to increase the splitting energies of the $n\pi^*$ states as well as the n cations. However, the splitting energies are still smaller than those predicted by the MO model (S CI or $\pi$ CI).

Finally, we consider the differences in the $^1n\pi^*$ and $^3n\pi^*$ states. Plots of the $\pi^*$ orbitals from the open shell HF calculations on the $^1n\pi^*$ and $^3n\pi^*$ states are shown in Figure

Table VII. Mulliken Populations for the $\pi^*$ Orbitals

| State | Excited N | Ortho C | Meta C | Para N |
|---|---|---|---|---|
| $^3n\pi^*$ | 0.333 | 0.170 | 0.024 | 0.279 |
| $^1n\pi^*$ | 0.100 | 0.110 | 0.026 | 0.628 |

3. As expected from considerations of the exchange integrals (cf. section II.B) the $\pi^*$ orbital in the $^1n\pi^*$ state localizes more on the para nitrogen, while the $\pi^*$ orbital in the $^3n\pi$ state has more density on the excited nitrogen and the ortho carbons. The conclusions drawn from the plots are confirmed by the Mulliken populations shown in Table VII.

Since the $\pi^*$ orbital is more localized for the $^1n\pi^*$ state, the splitting energy (between the $B_{3u}$ and $B_{2g}$ states) is expected to be smaller than that for the $^3n\pi^*$ states. The CI calculations bear out this expectation, although the difference in splitting energies is only 0.07 eV. Note that the MO model calculations (S·CI) predict the $^1n\pi^*$ splitting energy to be *larger* (~0.12 eV) than for $^3n\pi^*$, in direct contradiction to the VB model.

**(C) VB Model. Final Comments.** The calculations have shown conclusively that the VB model provides a more accurate description of the interaction of the n cation and $n\pi^*$ excited states. The excitations from the lone pairs are localized, although the nature of the pyrazine $\pi$ system leads to a delocalized $\pi^*$ orbital. The relatively large splitting of the n cations is explained by the slight delocalization of the nonbonding orbitals that allows them to become orthogonal to the $\sigma$ bonding orbitals (Pauli principle). We use the word slight, since Mulliken populations show that the nonbonding orbitals are still 90% localized on one nitrogen. The large splitting of the n cations is only slightly diminished in the $n\pi^*$ states because of the delocalized nature of the $\pi^*$ orbital.

In section II.A we stated that the Pauli-principle-induced delocalization of the nonbonding orbitals leads to a negative overlap of $n_l$ and $n_r$. Consequently, the $^2A_g$ and $^{1,3}B_{3u}$ states are stabilized relative to the $^2B_{1u}$ and $^{1,3}B_{2g}$, respectively. However, perusal of the plots in Figure 1 for the nonbonding orbitals from the $^2n$, $^1n\pi^*$, and $^3n\pi^*$ states reveals that the overlap of $n_l$ and $n_r$ is positive! At first, this appears to contradict both the VB model and the CI results. The real problem is that in the simple VB model we assumed that the $\sigma$ and $\pi$ electrons did not polarize in response to the lone pair excitation. This assumption allowed us to reduce the interaction of the two configurations $\Psi_L$ and $\Psi_R$ to a three- (or four-) electron problem and to show that the splitting energy is proportional to the overlap of $n_l$ and $n_r$. In the self-consistent calculations on the $^2n$, $^1n\pi^*$, and $^3n\pi^*$ states the $\sigma$ and $\pi$ electrons do polarize, so that one must consider the entire many-electron wave function for $\Psi_L$ and $\Psi_R$. In this case the overlap of $\Psi_L$ and $\Psi_R$ does not reduce to the overlap $n_l$ and $n_r$. Thus $\langle n_l | n_r \rangle$ may be positive for the self-consistent orbitals, while $\langle \Psi_L | \Psi_R \rangle$ is negative. The calculations prove that $\langle \Psi_L | \Psi_R \rangle$ is, in fact, negative.

We still have not shown that orthogonalization of the nonbonding orbitals to a *symmetric* $\sigma$ core will lead to the negative overlap assumed in the VB model. To check, we took the $n_+$ and $n_-$ orbitals used in the CI calculations and completely localized them by taking + and − combinations and zeroing all the coefficients for basis functions not on the left or right nitrogen, respectively. These localized "atomic like" lone pairs were orthogonalized to the symmetric $\sigma$ core. The resulting orbitals are plotted in Figure 4. Although it is difficult to tell from the plots, the actual overlap of $n_l$ and $n_r$ is −0.106 in agreement with the expectations of the VB model. The Mulliken populations for these orbitals are shown in Table VIII.

We may conclude that the assumption of a symmetric core in the VB model, although not rigorously correct, does not lead to incorrect conclusions. This is very gratifying since the assumption allows one to draw simple pictures and perform back-of-the-envelope calculations.

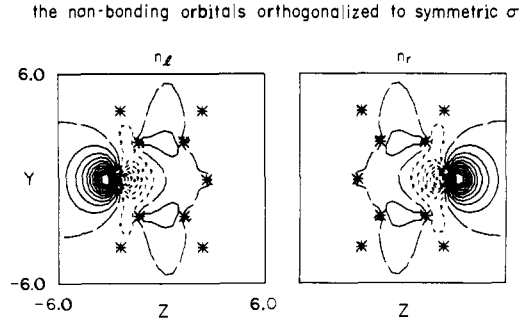


Figure 4. Contour plots of the $n_l$ and $n_r$ orbitals orthogonalized to a symmetric $\sigma$ core. The contour increment is 0.05 au.

Table VIII. Muliken Populations of the Atomic $n_l$ and $n_r$ Orbitals after Orthogonalization to the Symmetric $\sigma$ Core

| | | $n_l$ or $n_r$ |
|---|---|---|
| Excited N | s | 0.117 |
| | z | 0.832 |
| | Total | 0.949 |
| Ortho C | | 0.011 |
| Ortho H | | 0.008 |
| Meta C | | 0.025 |
| Meta H | | 0.001 |
| Para N | | 0.005 |

**Comparison with Experiment and Previous Calculations. (A) n Cations.** As mentioned in the Introduction, the MO model was very useful in interpreting the photoelectron spectrum of pyrazine. There are four bands below 12 eV in the photoelectron spectrum which are expected to correspond to the two n cations and the two lowest $\pi$ cations. The vertical ionization potentials occur at 9.63, 10.18, 11.35, and 11.77 eV.[25] Prior to the appearance of Hoffmann's[5] MO model, in which he predicted a large splitting (1-2 eV) of the n cations and that the $^2A_g$ state should be lower, these results would have been quite puzzling.

Nevertheless, the first four bands have been assigned in various ways: $\pi\pi nn$,[3] $\pi nn\pi$,[3] $n\pi n\pi$,[25,29] $\pi n??$,[26] $n\pi\pi n$,[27] $n\pi\sigma\pi$[28] (in increasing energy). Of these, the most reasonable is that of Gleiter, Heilbronner, and Hornung,[25] who assign the bands in increasing energy to $^2A_g(n)$, $^2B_{1g}(\pi)$, $^2B_{1u}(n)$, $^2B_{2g}(\pi)$. Their assignment is based on band shapes and is also supported by recent angular photoelectron work.[29] The first and third bands are peaked near the middle and resemble closely the two n cation bands in diazabicyclooctane (**12**).[30] The second and fourth bands are

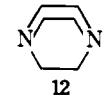

**12**

peaked at low energy, i.e., the vertical and adiabatic ionization energies coincide, and resemble the $\pi$ cation bands in benzene.[3] This assignment implies that the $\pi$ cations retain the ground state geometry, while the n cations change significantly.

Our results are the first ab initio calculations on the pyrazine cation. Previous theoretical estimates of the ionization potentials had been obtained using Koopmans' theorem in conjunction with semiempirical[5,25,31-33] or MBS ab initio[34-36] ground state HF wave functions. The results in Table IV show that Koopmans' theorem leads to ionization potentials for the n cations that are 2 to 3 eV too high and exaggerates the splitting by 1 eV. Therefore, none of the previous calculations of ionization potentials are reliable.

Table IX. Vertical Ionization Potentials (in eV)

| State | KT[a] | SCF | GVB CI[b] | π POL (2) CI | Exptl[c] |
|---|---|---|---|---|---|
| $^2A_g(n)$ | 12.03 | 11.32 | 10.27 | 10.01 | 9.63 |
| $^2B_{1g}(\pi)$ | 12.14 | 11.68 | 12.48 | 12.31 | 10.18 |
| $^2B_{1u}(n)$ | 14.70 | 13.55 | 11.70 | 11.51 | 11.35 |
| $^2B_{2g}(\pi)$ | 13.39 | | 13.36 | 13.16 | 11.77 |

[a] Koopmans' Theorem. [b] GVB CI: n−π CI for the n cations and π CI for the π cations. [c] Reference 25.

Table X. Size of the CI Calculations

| State | | GVB CI | π POL (2) CI | π POL (3) CI | HW[a] |
|---|---|---|---|---|---|
| $^1A_g$ | Configs[b] | 75 | 176 | 324 | 255 |
| | $\Delta E$[c] | 2.49 | 2.83 | 2.88 | 2.44 |
| $^1A_g$ | Configs | 42 | 75 | 139 | 255 |
| (π only)[d] | $\Delta E$ | 2.42 | 2.76 | 2.81 | 2.44 |
| $^1B_{3u}$ | Configs | 96 | 128 | 260 | 216 |
| | $\Delta E$ | 3.73 | 4.23 | 4.44 | 3.44 |

[a] Reference 36. [b] Spatial configurations. Each configuration yields one to six spin eigenfunctions and one to 20 determinants. [c] $\Delta E$ is the CI energy lowering relative to the single HF configuration (in eV). [d] Excitations are allowed only within the π space.

In Table IX, we list our results for both the n cations and the two lowest π cations, $^2B_{1g}$ and $^2B_{2g}$. Although the CI results for the n cations appear to support the nπnπ assignment,[25] especially when the $\sigma_{CC/CN}$ POL(1) CI results are considered, cf. Table IV, the calculated ionization potentials for the π cations are high by 1.5 to 2.0 eV. Since high quality CI wave functions are being employed, the only explanation for such a large error is the inflexible MBS employed. The high ionization energies indicate that the MBS exponents are too diffuse. As a result, the π electrons are not properly shielded by the σ core and so are too tightly bound. This problem has been corrected by using a double ζ basis and the resulting π ionization potentials (10.08 and 11.41) are in good agreement with experiment (10.18 and 11.77).[37]

(B) nπ* **Excited States.** The uv absorption, excitation, fluorescence, and phosphorescence spectra of pyrazine have been studied extensively.[2] Over the years the lowest energy singlet-singlet band system has often been analyzed in terms of a strong (allowed) n → π* transition to the $^1B_{3u}$ state and a weak (forbidden) n → π* transition usually thought to be the $^1B_{2g}$ state. The evidence for the second $^1$nπ* state has ranged from direct observation,[4,38-41] to indirect manifestations in the $^1B_{3u}$ bands such as vibronic line broadening[42] or electronic Coriolis interactions observed in the rotational structure.[43] The most recent spectroscopic studies show that the $^1B_{2g}$ state is higher than the $^1B_{3u}$.[44,45] Finally, none of the work on the $^3$nπ* states indicates the presence of the $^3B_{2g}$ state near the $^3B_{3u}$ state.[43-45]

From Tables V and VI we see that our calculations indicate that the $^{1,3}B_{2g}$ states are at least 1 eV higher than the $^{1,3}B_{3u}$ states. Therefore, if there is another state near the $^1B_{3u}$, it is not the $^1B_{2g}$. The experimental excitation energies of the $^1B_{3u}$ and $^3B_{3u}$ states are 3.2-3.3 and 3.8-3.9 eV, respectively.[2,47] Our n−π CI excitation energies are in reasonable agreement with experiment, being high by 0.1-0.3 eV, while the POL CI's lead to excitation energies that are too low by 0.1-0.3 eV. The singlet-triplet splitting is overestimated by 0.2 eV.

(C) **Comparison with Previous Theoretical Calculations.** The only previous ab initio study of the excited states of pyrazine was that of Hackmeyer and Whitten (HW).[36] They employed a basis set comparable to our MBS + DZ(π) and with the same geometry except that the CH bond lengths were taken as 1.05 Å[48] instead of 1.09 Å[49] as in our work. After performing an HF calculation on the ground state, they carried out CI calculations using the two lone pair orbitals, three occupied π orbitals, and six π* orbitals (two $b_{3u}$ and $a_u$, one $b_{2g}$ and $b_{1g}$) determined by IVO-type calculations (the $b_{1g}$ is determined by symmetry). The configurations were chosen by performing single and double excitations from one to three basic configurations, subjecting the generated configurations to an energy-lowering criterion, and repeating this process with the larger set of basic configurations. This procedure produces a set of configurations comparable to our π POL(3) CI.

In Table X, we list the number of configurations employed in the GVB CI,[50] π POL(2) CI, and π POL(3) CI as well as the energy lowerings for the $^1A_g$ and $^1B_{3u}$ states to contrast with the CI calculation of HW. We note that the smaller GVB CI leads to energy lowerings comparable to those of HW. Accordingly the π POL CI energy lowerings are significantly better than HW, although they involve a comparable number of configurations. Finally, we note that including the nonbonding orbitals in the CI calculations of the $^1A_g$ state decreases the energy by only 0.07 eV, while the number of configurations approximately doubles. This result supports the use of just the π space in the CI calculations on the ππ* states.

In Table XI we compare our CI results with those of HW and with experiment. Comparing the π POL(3) CI results with HW, we see that the nπ* excitation energies are, in general, 0.3 to 0.6 eV lower in the π POL(3) CI. The $B_{3u}/B_{2g}$ and $A_u/B_{1g}$(nπ*) state splitting energies are 0.1 to 0.3 eV smaller in the π POL(3) CI. The smaller splitting and excitation energies for the nπ* states in the π POL(3) CI relative to HW derive from the use by HW of the ground state HF $n_+$ and $n_-$ orbitals, which have extra σ character. Except for the ππ* states above 8 eV, the calculated excitations from HW and π POL(3) CI agree to ±0.05 eV for the ππ* states, as expected.

In both HW and the present work the excitation energies to the $1^1B_{1u}(\pi\pi^*)$ and $2^1B_{2u}(\pi\pi^*)$ states are overestimated by 2.5 to 3 eV. Extensive CI calculations by Hay and Shavitt[51] have shown that the analogous states in benzene have significant ionic character which leads to two problems in our calculations. First, the π orbitals would be expected to be a bit more diffuse than the normal valence excited states, requiring perhaps more diffuse functions than contained within the MBS + DZ(π) basis set. Second, one would expect significant readjustments among the σ orbitals in response to the ionic π system. With a minimal σ basis, the expected contraction effects are not allowed even in the $\sigma_{CC/CN}$ POL(1) CI and $\sigma_{CH}$ POL(1) CI calculations that allow σ readjustment.

Our π POL(3) CI calculations are in good agreement with experiment for both the $1^1B_{3u}$ and $1^3B_{3u}$ excitation energies. However, the excitation energies to the $1^3B_{1u}$ and $1^1B_{2u}(\pi\pi^*)$ states are high by 0.6 and 0.4 eV, respectively. This may again be a manifestation of the inflexibility of the MBS that we saw more dramatically in the case of the π cations.

Finally, we consider the question of the mystery state tentatively observed in the vicinity of the $^1B_{3u}(n\pi^*)$ state. Our calculations (vertical excitation energies) show only one state proximate to the $^1B_{3u}$, namely the $^3B_{1u}(\pi\pi^*)$ state (calculated separation 0.16 eV). Although the adiabatic energy of the $^3B_{1u}$ is known to be 0.5 eV lower than the adiabatic energy of the $^1B_{3u}$ state,[42] our calculations indicate that $^3B_{1u}$ and $^1B_{3u}$ potential surfaces cross (or are very close to each other) for configurations near the ground state geometry (at energies near 4 eV). Although the interaction of the states is spin forbidden, a strong spin-orbit interaction

Table XI. CI Results (eV)

| State | HF CI | S CI | GVB CI | $\pi$ POL(2) CI | $\pi$ POL(3) CI | Exptl[b] | HW |
|---|---|---|---|---|---|---|---|
| $1^1A_g$(GS) | 0.0[a] | 0.0[a] | 0.0[a] | 0.0[a] | 0.0[a] | | 0.0[a] |
| $1^3B_{3u}(n\pi^*)$ | 4.64 | 3.96 | 3.45 | 3.25 | 3.10 | 3.2–3.3 | 3.56 |
| $1^1B_{3u}(n\pi^*)$ | 5.47 | 4.94 | 4.23 | 4.07 | 3.91 | 3.8–3.9 | 4.22 |
| $1^3B_{1u}(\pi\pi^*)$ | 5.17 | 4.02 | 4.14 | 4.08 | 4.07 | 3.4–3.5[c] | 4.11 |
| $1^3B_{2g}(n\pi^*)$ | 6.64 | 5.83 | 4.70 | 4.56 | 4.41 | | 4.99 |
| $1^3A_u(n\pi^*)$ | 6.62 | 5.79 | 5.34 | 5.10 | 4.88 | | 5.14 |
| $1^1A_u(n\pi^*)$ | 6.76 | 5.79 | 5.37 | 5.12 | 4.90 | | 5.22 |
| $1^1B_{2g}(n\pi^*)$ | 7.75 | 7.09 | 5.38 | 5.30 | 5.12 | | 5.65 |
| $1^1B_{2u}(\pi\pi^*)$ | 8.68 | 6.49 | 5.41 | 5.34 | 5.26 | 4.8–4.9 | 5.29 |
| $1^3B_{2u}(\pi\pi^*)$ | 6.02 | 5.47 | 5.59 | 5.46 | 5.36 | | 5.39 |
| $2^3B_{1u}(\pi\pi^*)$ | 5.46 | 4.62 | 5.58 | 5.49 | 5.41 | | 5.41 |
| $1^3B_{1g}(n\pi^*)$ | 9.55 | 8.24 | 6.68 | 6.51 | 6.27 | | 6.89 |
| $1^1B_{1g}(n\pi^*)$ | 9.73 | 8.23 | 6.83 | 6.65 | 6.41 | | 7.04 |
| $2^1A_g(n\pi^*)$[d] | | | 6.97 | 7.03 | 6.54 | | 7.33 |
| $3^3B_{1u}(n\pi^*)$[d] | | | 7.33 | 7.41 | 6.93 | | 7.73 |
| $1^3A_g(\pi\pi^*)$ | 10.53 | 9.98 | 7.80 | 7.80 | 7.67 | | 7.64 |
| $1^3B_{3g}(\pi\pi^*)$ | 11.19 | 10.90 | 7.88 | 7.85 | 7.73 | | 7.79 |
| $2^3B_{2g}(n\pi^*)$ | | | 8.33 | 8.27 | 7.93 | | 8.31 |
| $2^1B_{2g}(n\pi^*)$ | | | 8.47 | 8.42 | 8.09 | | 8.47 |
| $2^3B_{2u}(\pi\pi^*)$ | 7.45 | 6.92 | 9.20 | 8.72 | 8.62 | | 8.38 |
| $3^1A_g(\pi\pi^*)$ | 13.55 | 13.18 | 9.04 | 9.04 | 8.85 | | |
| $1^1B_{3g}(\pi\pi^*)$ | 13.55 | 12.70 | 9.04 | 9.01 | 8.90 | | |
| $2^3B_{3g}(\pi\pi^*)$ | | | 9.44 | 9.42 | 9.11 | | |
| $1^1B_{1u}(\pi\pi^*)$ | 9.69 | 9.48 | 9.87 | 9.41 | 9.31 | 6.5–6.6 | 9.10 |
| $2^1B_{3u}(n\pi^*)$ | | | 9.64 | 9.65 | 9.34 | | |
| $2^1B_{2u}(\pi\pi^*)$ | 10.05 | 7.94 | 10.93 | 10.52 | 10.36 | 7.6–7.7 | 9.95 |

[a] The ground state energies (au) from left to right are −261.95270, −261.95270, −262.04408 (−262.04180), −262.05674 (−262.05421), −262.05872 (−262.05613), −262.3579. The CI energies in which only the $\pi$ space was used are listed parenthetically. [b] References 2 and 47. [c] Reference 42 (adiabatic excitation energy). [d] Dominant configurations involve a double excitation, $n \rightarrow \pi^*$, $n \rightarrow \pi^*$.

Table XII. Singlet Rydberg Adiabatic Excitation Energies (eV)

| State | $^1A_g$ core | $^2$n core | $^2B_{1g}$ core | Exptl[a] | $f$calcd[b] |
|---|---|---|---|---|---|
| $^1A_g\ n_+(a_g) \rightarrow 3s$ | 6.60 | 6.58 | | | |
| $^1B_{2u} \rightarrow 3p_y$ | 7.23 | 7.13 | | 6.84 | $7.33 \times 10^{-3}$ |
| $^1B_{3u} \rightarrow 3p_x$ | 7.32 | 7.33 | | | $1.98 \times 10^{-5}$ |
| $^1B_{1u} \rightarrow 3p_z$ | 7.38 | 7.41 | | 6.75 | $9.22 \times 10^{-4}$ |
| $^1A_g \rightarrow 3d_{y^2}$[c] | 7.72 | 7.74 | | | |
| $^1B_{3g} \rightarrow 3d_{yz}$ | 7.93 | 7.92 | | | |
| $^1B_{2g} \rightarrow 3d_{xz}$ | 8.06 | 8.11 | | | |
| $^1B_{1g} \rightarrow 3d_{xy}$ | 8.08 | 8.06 | | | |
| $^1A_g \rightarrow 3d_{z^2}$[c] | 8.17 | 8.23 | | | |
| $^1B_{1g}\ \pi(b_{1g}) \rightarrow 3s$ | 7.27 | | 7.39 | | |
| $^1B_{3u} \rightarrow 3p_y$ | 7.87 | | 7.88 | | $5.52 \times 10^{-3}$ |
| $^1B_{2u} \rightarrow 3p_x$ | 8.13 | | 8.24 | | $7.57 \times 10^{-3}$ |
| $^1A_u \rightarrow 3p_z$ | 8.30 | | 8.31 | | |
| $^1B_{1g} \rightarrow 3d_{y^2}$[c] | 8.39 | | 8.46 | | |
| $^1B_{2g} \rightarrow 3d_{yz}$ | 8.76 | | 8.75 | | |
| $^1A_g \rightarrow 3d_{xy}$ | 8.82 | | 8.84 | | |
| $^1B_{3g} \rightarrow 3d_{xz}$ | 8.92 | | 8.95 | | |
| $^1B_{1g} \rightarrow 3d_{z^2}$[c] | 9.15 | | 9.18 | | |

[a] Reference 54. [b] $f$calcd is the (dipole) oscillator strength calculated using IVO's obtained with the $^1A_g$ core. [c] The $3d_{2z^2-x^2-y^2}$ and $3d_{x^2-y^2}$ orbitals are not properly described since the diffuse functions were partitioned into $\sigma$ and $\pi$ sets.

is expected between the two states.[52] Therefore, in the advent of near degeneracy of the $^1B_{3u}$ and $^3B_{1u}$ potential surfaces, the $^3B_{1u}$ state is a plausible origin of the perturbations observed in the $^1B_{3u}$ bands.

**(D) Rydberg States. (1) Excitation Energies.** In the previous section, we ruled out the possibility of another $^1n\pi^*$ or $^1\pi\pi^*$ state being in the vicinity of the $^1B_{3u}$ state. However, there is a possibility that the lowest Rydberg singlet state, namely the $^1A_g(n \rightarrow 3s)$ state, is near the $^1B_{3u}$ state. At first, this sounds preposterous in light of the vacuum uv work of Parkin and Innes (PI)[53] and Scheps, Florida, and Rice (SFR)[54] who observed the lowest allowed Rydberg singlet (presumably $n \rightarrow 3p$) at 6.75 eV. However, in water the $^1B_1(\pi \rightarrow 3s)$ Rydberg state is 2.5 eV lower than the $^1B_1(\pi \rightarrow 3p_z)$ state. The large separation arises from the fact that the OH bonds in water are strongly polarized toward the oxygen so that the electron in the 3s orbital "sees" the protons; the 3s orbital tightens and lowers the energy.[16,17] Therefore, we calculated the energies of the lowest Rydberg states in pyrazine using the IVO method,[16] which has been successfully applied to water.[16,17] Singlet excitation energies were calculated for the lowest Rydberg states arising from excitation of an electron from either a nonbonding orbital or the most loosely bound $\pi$ orbital. The IVO calculation yields directly the stability (ionization potential) of the excited (Rydberg) orbitals; to obtain excitation energies, we subtract the stability of the Rydberg orbital from the experimental adiabatic ionization potential[16] (9.28 eV for n and 10.11 for $\pi$).[3] This procedure assumes that the potential surfaces of the Rydberg state and appropriate cation are similar, so that the differences in the adiabatic and vertical excitation energies are the same.

The results of the IVO calculations are given in Table XII. Two sets of calculations were made, one using a

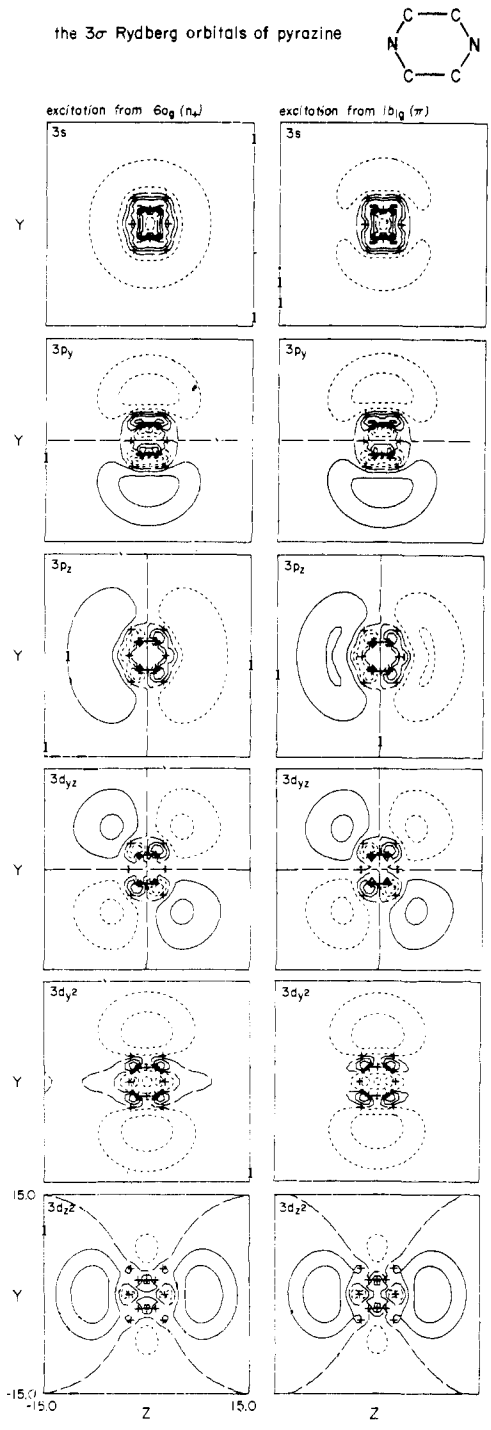


**Figure 5.** Contour plots of the pyrazine 3σ Rydberg orbitals excited from the $6a_g(n_+)$ and $1b_{1g}(\pi)$ orbitals. The contours are: 0.0, ±0.01, ±0.02154, ±0.04641, ±0.1, etc.

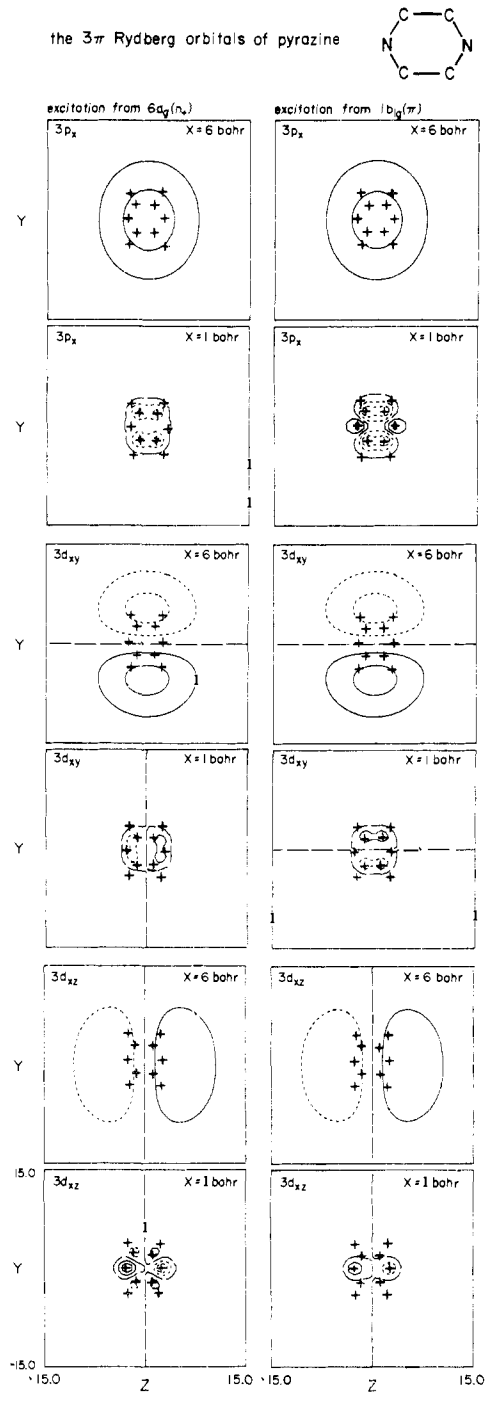


**Figure 6.** Contour plots of the pyrazine 3π Rydberg orbitals excited from the $6a_g(n_+)$ and $1b_{1g}(\pi)$ orbitals. The contours are: 0.0, ±0.01, ±0.02154, ±0.04641, ±0.1, etc.

ground state core and the other using the appropriate cation core ($^2$n or $^2B_{1g}$). The calculated stabilities of the Rydberg orbitals are seen to be relatively insensitive to the type of core. This is a manifestation of the inflexibility of the MBS in that the cation orbitals cannot contract relative to the neutral orbitals. Using the $^2$n core instead of the $^1A_g$ core for the n Rydberg states is more correct in that the excitation is then described as being localized. Although the Rydberg orbitals are shifted toward the excited nitrogen when the $^2$n cation is used, the actual stability of each orbital is affected only slightly.

Analyzing the vacuum uv spectrum of pyrazine, SFR[54] interpreted the bands in terms of two Rydberg series, one weak and one strong, both converging to 9.28 eV. The electronic origins for the lowest members of the series were observed at 6.75 eV (weak) and 6.84 eV (strong). SFR assigned the weak band to the $^1B_{3u}[\pi(b_{1g}) \rightarrow 3p_y]$ state and the strong band to the $^1B_{2u}[\pi(b_{1g}) \rightarrow 3p_x]$ state. They rejected the possible assignment as n → 3p on the basis that this would lead to three allowed transitions from the $n_+(a_g)$ orbital [namely, $n_+(a_g) \rightarrow 3p_x$ (weak), $n_+(a_g) \rightarrow 3p_y$ (weak), and $n_+(a_g) \rightarrow 3p_z$ (strong)], whereas only two are observed. Moreover, their assignment of the strong band as due to a $^1B_{2u}$ state was supported by the rotational contour analysis of PI.[53]

These assignments of the Rydberg state indicate that the lowest ionization in pyrazine involves a π electron in agree-

Table XIII. Size of Pyrazine and Water Rydberg Orbitals

| | Pyrazine $n_+$ ($a_g$) | | | Pyrazine $\pi$ ($b_{1g}$) | | | Water $\pi$ ($1b_1$) | | |
|---|---|---|---|---|---|---|---|---|---|
| Orbital | $\langle x^2\rangle$ | $\langle y^2\rangle$ | $\langle z^2\rangle$ | $\langle x^2\rangle$ | $\langle y^2\rangle$ | $\langle z^2\rangle$ | $\langle x^2\rangle$ | $\langle y^2\rangle$ | $\langle z^2\rangle$ |
| 3s | 21.713 | 20.242 | 18.013 | 21.874 | 21.146 | 12.940 | 5.079 | 7.578 | 8.548 |
| $3p_x$ | 44.325 | 18.828 | 13.929 | 44.738 | 18.947 | 14.186 | 42.959 | 14.320 | 15.372 |
| $3p_z$ | 13.055 | 56.546 | 14.081 | 12.828 | 54.067 | 12.396 | 5.230 | 16.549 | 6.996 |
| $3p_z$ | 15.830 | 23.696 | 51.020 | 16.955 | 27.335 | 47.481 | 14.850 | 15.443 | 28.148 |
| $3d_{xy}$ | 39.079 | 41.358 | 13.876 | 39.114 | 41.376 | 13.887 | | | |
| $3d_{xz}$ | 42.909 | 20.746 | 40.095 | 45.219 | 22.249 | 41.671 | 56.508 | 18.836 | 52.843 |
| $3d_{yz}$ | 14.839 | 49.539 | 40.529 | 15.009 | 51.050 | 39.720 | 19.466 | 58.504 | 24.847 |
| $3d_{y^2}$ | 17.827 | 51.327 | 10.449 | 17.929 | 46.766 | 9.940 | 29.149 | 71.700 | 20.334 |
| $3d_{z^2}$ | 15.131 | 13.764 | 51.865 | 12.199 | 13.185 | 60.712 | 39.382 | 19.725 | 68.460 |
| 4s | | | | | | | 48.006 | 36.288 | 60.571 |
| $4p_x$ | | | | | | | 254.068 | 89.689 | 86.209 |
| $4p_y$ | | | | | | | 30.259 | 90.321 | 59.605 |
| $4p_z$ | | | | | | | 81.665 | 80.579 | 184.486 |
| $4d_{xy}$ | | | | | | | | | |
| $4d_{xz}$ | | | | | | | 79.908 | 239.756 | 87.682 |
| $4d_{yz}$ | | | | | | | | | |
| $4d_{y^2}$ | | | | | | | | | |
| $4d_{z^2}$ | | | | | | | | | |

ment with the photoionization work,[55] but in conflict with the photoelectron work.[25,29] Since our n-cation calculations[56] are in agreement with the photoelectron results, we have assumed in calculating the energies in Table XI that the lowest ionization involves the n cation. We also find support for this assumption in the Rydberg spectra. SFR observed that the pyrazine Rydberg series has much richer vibrational structure than the Rydberg series in benzene. This indicates a substantial change in the geometry of pyrazine between the ground state and the Rydberg states, while there is little change in benzene.[54] This difference is consistent with the idea that the pyrazine Rydberg states involve an excitation out of an n orbital, while the benzene Rydberg states involve an excitation out of a $\pi$ orbital.

The IVO calculations predict the three n $\rightarrow$ 3p transitions to be within 0.15 eV of one another, in qualitative agreement with SFR.[54] However, the calculated oscillator strengths are very different from what one might expect. The $n_+ \rightarrow 3p_z$ is not the strongest transition, but rather the $n_+ \rightarrow 3p_y$. The relative intensities of the $n_+ \rightarrow 3p_y$, $n_+ \rightarrow 3p_z$, and $n_+ \rightarrow 3p_x$ are calculated to be 370:47:1. There are two important ramifications of this result. (1) The strongest observed transition, n $\rightarrow 3p_y$, is $y$ polarized in agreement with the rotational contour analysis of PI.[53] (2) The n $\rightarrow 3p_x$ transition is so weak that it would be very difficult to observe. Therefore, the observation of only two transitions by SFR[54] is understandable.

SFR[54] observed the electronic origin of the weak band (n $\rightarrow 3p_z$) 0.09 eV below that of the strong band (n $\rightarrow 3p_y$), while the IVO calculations lead to the n $\rightarrow 3p_z$ transition 0.15 eV higher than the n $\rightarrow 3p_y$. However, the calculated excitation energies are all too high by 0.5 eV, probably because of the inflexibility of the MBS description of the core (not allowing contraction of the $\sigma$ orbitals). Therefore, errors in the calculated excitation energies of 0.24 eV are not unreasonable. On the other hand, it is also possible that the origin of the *weak* $n_+ \rightarrow 3p_z$ transition was misassigned.

Finally, our calculations indicate that the relatively strong $\pi(b_{1g}) \rightarrow 3p_x$ and $\pi(b_{1g}) \rightarrow 3p_y$ transitions should be observed 0.6 to 0.8 eV above the set of n $\rightarrow$ 3p transitions, i.e., near 7.5 eV. However, the very strong $\pi \rightarrow \pi^*$ transition to the $2^1B_{2u}$ state occurs in this region and so it would be difficult to abstract these Rydberg transitions from the spectrum.

**(2) Nature of Rydberg Orbitals.** The $\sigma$ Rydberg orbitals,[57] obtained by exciting from the $n_+(a_g)$ and $\pi(b_{1g})$ orbitals, are plotted (in the molecular plane) in Figure 5. For the $\pi$ Rydberg orbitals[57] (Figure 6) plots are made 1 and 6 bohr above the molecular plane. Comparing the Rydberg orbitals from the $n_+$ and $\pi$ orbitals, we see that they are quite similar, except that there is greater electron density near the nitrogens for $\sigma$ Rydbergs excited from the $n_+$ orbital. The greater density is a manifestation that the Rydberg orbital has to get orthogonal (Pauli principle) to only one nitrogen lone pair instead of two.

We have been labeling these Rydberg states with a principal quantum number of 3. However, this designation is not consistent with the atomic concept that $n = 3$ orbitals have two nodes. The Rydberg orbitals must get orthogonal to the core orbitals (Pauli principle). For the $\sigma$ Rydberg orbitals two spherical nodal planes (diagramed below) are required for orthogonality to the $\sigma$ core. As is apparent from the plots, these nodal planes are always present whether the orbital is an s, p, or d. Thus, the s orbital has two nodal planes, the $p_\sigma$ three, and the $d_\sigma$ four. Consequently, assigning principal quantum numbers according to the number of nodal planes would not indicate the basic character of these orbitals. A better scheme is to group the orbitals according to size. In Table XIII we compare the sizes of the pyrazine Rydberg orbitals with the $n = 3$ and $n = 4$ Rydberg orbitals of water,[17] using the expectation values $\langle x^2\rangle$, $\langle y^2\rangle$, and $\langle z^2\rangle$ to measure size. Plots of the 3s and $3p_z$ orbitals for $H_2O$ (excited from either the $n(a_1)$ or $\pi(b_1)$ orbital) are also shown in Figure 7 for comparison. The pyrazine orbitals are clearly comparable in size to the $n = 3$ water orbitals.

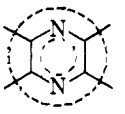


In passing, we note that the $\pi$ Rydberg orbitals in pyrazine require only one nodal plane to become orthogonal to the core, so that no corresponding ambiguity occurs.

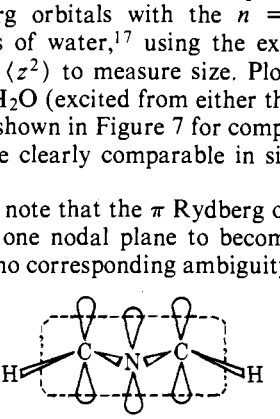


**(E) Relationship of the $n\pi^*$ and $\pi\pi^*$ States.** In Figure 8, we compare the spectra of $n\pi^*$ and $\pi\pi^*$ excited states for pyrazine. Previously we considered the lowest $n\pi^*$ states, namely $1^{1,3}B_{3u}$ and $1^{1,3}B_{2g}$. In these states, the $\pi^*$ orbital has $b_1$ symmetry (for the $C_{2v}$ group) as is evident from the plots in Figures 3 and 4. Another higher lying set of $n\pi^*$ states ($A_u$ and $B_{1g}$) is obtained in which the $\pi^*$ orbital is of

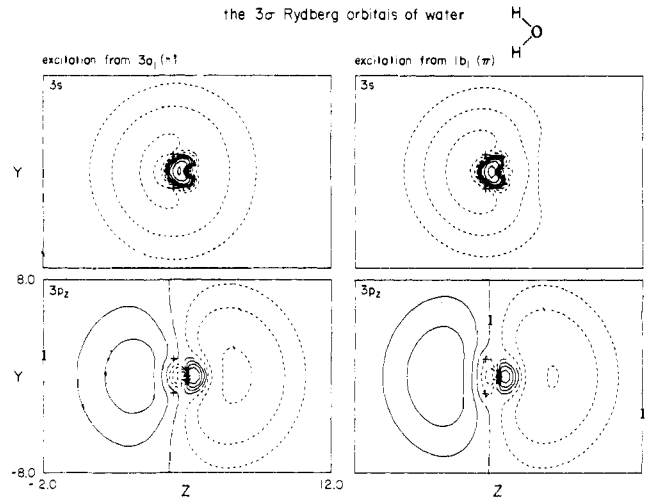


Figure 7. Contour plots of the water 3s and $3p_z$ Rydberg orbitals excited from the 3a(n), and $1b_1(\pi)$ orbitals. The contours are: p.0, ±0.01, ±0.02154, ±0.04641, ±0.1, etc.

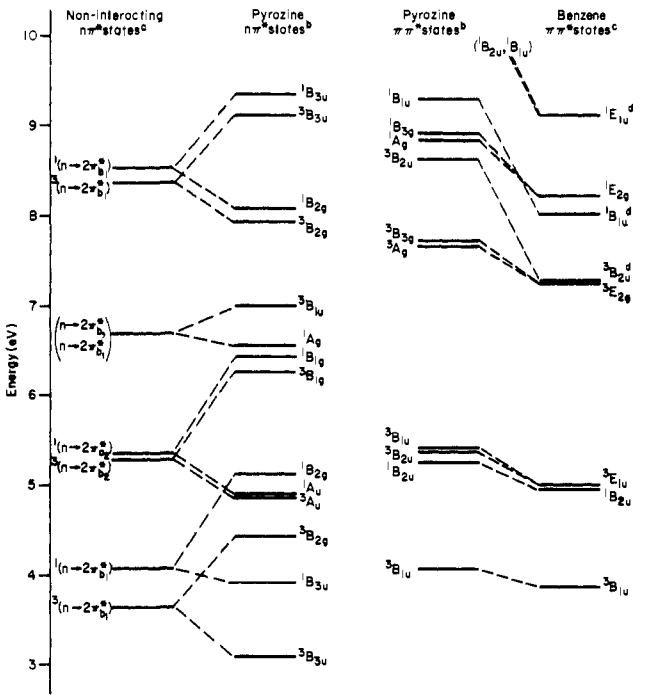


Figure 8. Energy level diagram for the nπ* and ππ* states of pyrazine. Footnotes: (a) SCF calculations with relaxed symmetry ($C_{2v}$). Only the lowest two levels are based on actual calculations. The other levels represent educated guesses; (b) π POL(3) CI energies; (c) π POL(3) CI energies from ref 58; (d) these states are ionic in character and may not be well described by a double ζ basis.[51]

$a_2$ symmetry, i.e., with a node through the nitrogens. These $b_1\pi^*$ and $a_2\pi^*$ orbitals of pyrazine correspond to the $e_u\pi^*$ orbital of benzene. In contradistinction to the case of the $b_1\pi^*$ orbital, the $a_2\pi^*$ orbital cannot localize on the excited nitrogen to maximize the favorable exchange interaction in the triplet (nor localize on the para nitrogen to minimize the bad exchange interaction in the singlet). As a result the singlet-triplet splittings in the $A_u$ and $B_{1g}$ states are ~0.1 eV compared to ~0.75 eV for the $B_{3u}$ and $B_{2g}$ states.

The third set of nπ* states involves the second $b_1\pi^*$ orbital (corresponding to $a_{2g}\pi^*$ of benzene), but the ordering of the $B_{2g}$ and $B_{3u}$ states is reversed, with the $B_{2g}$ lower. The reversal in state ordering arises from the fact that the second $b_1\pi_r^*$ and $\pi_l^*$ orbitals have a negative overlap (induced by the Pauli principle), while the opposite was true for the lowest b, π*, and $\pi_l^*$ orbitals (cf. section II.B).

Finally, there are two nπ* states ($^1A_g$ and $^3B_{1u}$) that involve a *double* excitation. The VB picture for these states is shown below and reveals a σ system like that of 1,4-benzyne. The two unpaired n orbitals can be singlet or tripled coupled leading to $2^1A_g$ and $2^3B_{1u}$ states, respectively. Because of the Pauli-induced coupling of the $n_l$ and $n_r$ orbitals, the singlet state should be lower; the calculated singlet-triplet splitting is 0.30 eV. The excitation energies to the $2^1A_g$ and $2^3B_{1u}$ states are approximately twice that for the $1^{1,3}B_{3u}$, as would be expected from **13**.

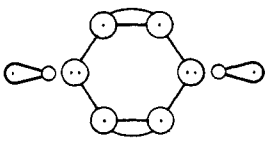

**13**

For the ππ* states we have compared the excitation energies to those of benzene (using comparable CI calculations, that is, POL(3) CI with a valence double ζ basis for the π system).[58] The calculations on benzene employed a double ζ basis for the σ core, so that the description of the benzene σ core is much more accurate than the MBS description of the pyrazine σ core. Consequently, all the benzene ππ* states are calculated at lower energies and it is difficult to make any quantitative statements concerning the effect of the nitrogens. However, it is interesting to note that the doubly-degenerate $^3E_{1u}$, $^3E_{2g}$, and $^1E_{2g}$ states of benzene are split by only 0.1 eV or less in pyrazine.

## VII. Summary

We have proposed a VB model for describing the n cations and nπ* states of pyrazine. The n cations and nπ* states are described by a resonant (or antiresonant) combination of two equivalent configurations which describe either an n ionization or an n to π promotion localized on one of the nitrogens. The splitting energy of the resonant and antiresonant wave functions is proportional to the overlap (or product of overlaps) of the singly-occupied orbitals, i.e., $\Delta E \propto \langle n_l | n_r \rangle$ for the n cations and $\Delta E \propto \langle n_l | n_r \rangle \langle \pi_l^* | \pi_r^* \rangle$ for the nπ* states. The orthogonalization of the n orbitals to the σ core mandated by the Pauli principle leads to a negative overlap for $n_l$ and $n_r$, but a positive overlap for $\pi_l^*$ and $\pi_r^*$. Consequently, the $^2A_g$ and $^{1,3}B_{3u}$ states are stabilized with respect to the $^2B_{1u}$ and $^{1,3}B_{2g}$ states, respectively. Finally, although the n → π promotion is localized on one nitrogen, the resulting π* orbital is delocalized because of the nature of the benzene-like π system. Thus, the splitting energy of the nπ* states is predicted to be only slightly smaller (~⅔ the size) than the n cation splitting.

Ab initio MBS CI calculations show that the VB model affords a more accurate description of the n cations and nπ* states than the MO model,[4] which leads to errors of 1.5 to 2 eV. The nonbonding orbitals are actually quite localized (90% on one nitrogen), in contradistinction to the delocalized symmetry orbitals of the MO model.

Comparison of our results on the n cations with experiment confirms the photoelectron assignments of Gleiter, Heilbronner, and Hornung,[25] namely $^2A_g(n)$, $^2B_{1g}(\pi)$, $^2B_{1u}(n)$, $^2B_{2g}(\pi)$ in order of increasing energy. The calculated splitting of the n cations is 1.64 eV; the experimental value is 1.72 eV. We found that an MBS leads to a poor description of the π cations.

Finally, the assignment of the lowest ionization potential to the n orbital implies that the previous assignments of the Rydberg series[52,53] in terms of $\pi(B_{1g}) \rightarrow np$ excitations are incorrect. Assuming that the lowest ionization is from an n

orbital, our IVO[16] Rydberg calculations show that the strong transition observed at 6.84 eV corresponds to $n_+ \rightarrow 3p_y(^1B_{2u})$, while the weak transition observed at 6.75 eV corresponds to $n_+ \rightarrow 3p_z(^1B_{1u})$. The $n_+ \rightarrow 3p_x(^1B_{3u})$ transition is calculated to be ~50 times weaker than the $n_+ \rightarrow 3p_z$ and, thus, the observation of only one weak band is not surprising, although a search for the other weak band is warranted.

Analysis of the pyrazine Rydberg orbitals reveals that they should be classified as to principal quantum number according to their size rather than the number of nodal planes. We find that two spherical nodal planes are required for $\sigma$ Rydberg orbitals to be orthogonal to the core, while only one node is required for $\pi$ Rydberg orbitals.

**Acknowledgment.** This work was aided by a grant (GP-40783X) from the National Science Foundation. We thank Dr. Thom H. Dunning, Jr., Professor William Moomaw, and Dr. Nicholas Winter for many stimulating conversations.

## References and Notes


(1) NSF Predoctoral Fellow, 1970–1973; California Institute Research Foundation Fellow, 1973–1974.
(2) K. K. Innes, J. P. Byrne, and I. G. Ross, *J. Mol. Spectrosc.*, **22**, 125 (1967), and references cited therein.
(3) D. W. Turner, C. Baker, A. D. Baker, and C. R. Brundle, "Molecular Photoelectron Spectroscopy," Interscience, New York, N.Y., 1970.
(4) M. A. El-Sayed and G. W. Robinson, *Mol. Phys.*, **4**, 273 (1961).
(5) (a) R. Hoffmann, A. Imamura, and W. J. Hehre, *J. Am. Chem. Soc.*, **90**, 1499 (1968); (b) R. Hoffmann, *Acc. Chem. Res.*, **4**, 1 (1971).
(6) The $\pi$ electrons have been suppressed for the moment, while the hydrogens will be suppressed throughout the paper.
(7) The self-consistent wave functions for the $\Psi(^2A_g)$ or $\Psi(^2B_{1u})$ states lead to doubly-occupied $\sigma$ and $\pi$ orbitals that are polarized toward the singly-occupied nonbonding orbital. (See the section Calculational Details.) Therefore, $\Phi_{core}$ is not the same for both $\Psi_L$ and $\Psi_R$ and $S = \langle\Psi_L|\Psi_R\rangle \neq -\langle n_l|n_r\rangle$. Also, the singly-occupied nonbonding orbital will be contracted relative to the doubly-occupied lone pair. The upshot of all this is that eq 6 cannot be reduced to (7). The splitting energy cannot be analyzed in terms of a simple three-electron problem or shown to be proportional to overlap of $n_l$ and $n_r$. However, the results indicate that our simple VB model is in accord with more accurate but much more involved descriptions.
(8) $\Psi_L$ and $\Psi_R$ are not actually normalized since $\langle\Psi_L|\Psi_L\rangle = \langle\mathcal{A}[(\Phi_{core})n_r^2n_l\alpha\beta\cdots\alpha\beta]|\mathcal{A}[(\Phi_{core})n_r^2n_l\alpha\beta\cdots\alpha\beta]\rangle$. All the orbitals in $\Phi_{core}$ are orthogonal to one another and to $n_r$ and $n_l$, so that $\langle\Psi_L|\Psi_L\rangle = \langle\mathcal{A}(n_r^2n_l\alpha\beta\alpha)|\mathcal{A}(n_r^2n_l\alpha\beta\alpha)\rangle$. All the terms vanish by spin orthogonality except those involving interchange of electrons 1 and 3 or no interchange at all, so that $\langle\Psi_L|\Psi_L\rangle = 1 - \langle n_l|n_r\rangle^2 \equiv 1 - S_{lr}^2$. Therefore, we assume that the normalization factor of $1/\sqrt{1 - S_{lr}^2}$ is included in the antisymmetrizer.
(9) Substituting (3) and (4) into $S = \langle\Psi_L|\Psi_R\rangle$ gives $\langle\Psi_L|\Psi_R\rangle = [1/(1 - S_{lr}^2)]\langle\mathcal{A}(n_r^2n_l\alpha\beta\alpha)|\mathcal{A}(n_l^2n_r\alpha\beta\alpha)\rangle$. As in ref 8, all the terms vanish except those involving interchange of electrons 1 or 3 or no interchange at all, so that $\langle\Psi_L|\Psi_R\rangle = [1/(1 - S_{lr}^2)](S_{lr}^3 - S_{lr})$ or $\langle\Psi_L|\Psi_R\rangle = -S_{lr}$.
(10) Evaluating the two-electron part of (6) gives $\Delta E(2e^-) = 2(3S_{lr}K_{lr} - S_{lr}J_{lr}) + 2S_{lr}(J_{ll} + 2J_{lr} - K_{lr}) = 2S_{lr}(J_{ll} + J_{lr} + 2K_{lr})$. The $S_{lr}J_{ll}$ term is the largest but is obviously dominated by $S_{lr}h_{ll}$ which appears in the one-electron part of (6).
(11) (a) C. W. Wilson, Jr., and W. A. Goddard III, *Chem. Phys. Lett.*, **5**, 45 (1970); (b) *Theor. Chim. Acta*, **26**, 195, 211 (1972).
(12) T. Koopmans, *Physica*, **1**, 104 (1934).
(13) (a) S. L. Guberman and W. A. Goddard III, *Chem. Phys. Lett.*, **14**, 460 (1972); (b) D. L. Huestis and W. A. Goddard III, *ibid.*, **16**, 157 (1972); (c) W. A. Goddard III, T. H. Dunning, Jr., W. J. Hunt, and P. J. Hay, *Acc. Chem. Res.*, **6**, 368 (1973).
(14) W. J. Hunt, W. A. Goddard III, and T. H. Dunning, Jr., *Chem. Phys. Lett.*, **6**, 147 (1970).
(15) The CI calculations reported in section V employed unprojected $n_+$ and $n_-$ orbitals. The effect of projection is relatively minor (excitation energies change by at most 0.2 eV), but, in general, projection leads to lower absolute energies in the CI calculations by 3 to 8 mhartrees.
(16) S. Huzinaga, D. McWilliams, and B. Dansky, *J. Chem. Phys.*, **54**, 2283 (1971).
(17) T. H. Dunning, Jr., private communication. The 7s primitives were contracted 5s, 3s.
(18) The six 1s core orbitals were always forced to be doubly occupied and were taken from the HF calculation on the ground state.
(19) W. J. Hunt and W. A. Goddard III, *Chem. Phys. Lett.*, **3**, 414 (1969).
(20) W. A. Goddard III and W. J. Hunt, *Chem. Phys. Lett.*, **24**, 464 (1974).
(21) D. C. Cartwright, W. J. Hunt, W. Williams, S. Trajmar, and W. A. Goddard III, *Phys. Rev. A*, **8**, 2436 (1973).
(22) The absolute energy of the $^1A_g$ state in the n–$\pi$ CI decreases by only 0.07 eV relative to the $\pi$ CI.
(23) There is another independent spin eigenfunction that can be found from this configuration. However, we consider just the one that makes the largest contribution to the CI wave function.
(24) The decrease in $\pi$ correlation energy when a seventh electron is added may at first seem unreasonable. However, in the seven-electron $\pi$ system, one of the $p_\pi$ orbitals is doubly occupied (cf **5**) so that there are only five singly-occupied $p_\pi$ orbitals. Since the correlation energy of the singly-occupied $p_\pi$ orbitals is much greater than that of the doubly-occupied $p_\pi$ orbital, the ground state with six singly-occupied $p_\pi$ orbitals is expected to have a larger $\pi$ correlation energy.
(25) R. Gleiter, E. Heilbronner, and V. Hornung, *Angew. Chem.*, **82**, 878 (1970); *Helv. Chim. Acta*, **55**, 255 (1972).
(26) M. J. S. Dewar and S. D. Worley, *J. Chem. Phys.*, **51**, 263 (1969).
(27) K. A. Muszkat and J. Schäublein, *Chem. Phys. Lett.*, **13**, 301 (1972).
(28) C. Fridh, L. Åsbrink, B. O. Jonsson, and E. Lindholm, *Int. J. Mass Spectrom. Ion Phys.*, **8**, 101 (1972).
(29) D. L. Ames, J. P. Maier, F. Watt, and D. W. Turner, *Faraday Discuss. Chem. Soc.*, **54**, 277 (1972).
(30) E. Heilbronner and K. A. Muszkat, *J. Am. Chem. Soc.*, **92**, 3818 (1970).
(31) (a) T. Yonezawa, H. Yamabe, and H. Kato, *Bull. Chem. Soc. Jpn.* **42**, 76 (1969); (b) T. Yonezawa, H. Kato, and H. Kato, *Theor. Chim. Acta*, **13**, 125 (1969).
(32) M. Sundboom, *Acta Chem. Scand.*, **25**, 487 (1971).
(33) R. L. Ellis, G. Kuehnlenz, and H. H. Jaffe, *Theor. Chim. Acta*, **26**, 131 (1972).
(34) E. Clementi, *J. Chem. Phys.*, **46**, 4737 (1967).
(35) J. D. Petke, J. L. Whitten, and J. A. Ryan, *J. Chem. Phys.*, **48**, 953 (1968).
(36) M. Hackmeyer and J. L. Whitten, *J. Chem. Phys.*, **54**, 3739 (1971).
(37) W. R. Wadt, W. A. Goddard III, and T. H. Dunning, Jr., to be published.
(38) M. Ito, R. Shimada, T. Kuraishi, and W. Mizushima, *J. Chem. Phys.*, **26**, 1508 (1957).
(39) M. A. El-Sayed and G. W. Robinson, *J. Chem. Phys.*, **34**, 1840 (1961); **35**, 1896 (1961).
(40) The vapor spectrum of 2,6-dimethylpyrazine was interpreted in terms of a second forbidden $n\pi^*$ state.
(41) W. R. Moomaw, M. R. DeCamp, and P. C. Podore, *Chem. Phys. Lett.*, **14**, 255 (1972).
(42) R. M. Hochstrasser and C. Marzzacco, *J. Chem. Phys.*, **49**, 971 (1968).
(43) K. K. Innes, A. H. Kalantar, A. Y. Khan, and T. J. Durnick, *J. Mol. Spectrosc.*, **43**, 477 (1972).
(44) C. J. Marzzacco and E. F. Zalewski, *J. Mol. Spectrosc.*, **43**, 239 (1972).
(45) H.-K. Hong and G. W. Robinson, *J. Mol. Spectrosc.*, **52**, 1 (1974).
(46) W. R. Moomaw and M. A. El-Sayed, *J. Chem. Phys.*, **45**, 3890 (1966); **48**, 2502 (1968).
(47) M. N. Pisanias, L. G. Christophorou, J. G. Carter, and D. L. McCorkle, *J. Chem. Phys.*, **58**, 2110 (1973).
(48) P. J. Wheatley, *Acta Crystallogr.*, **10**, 182 (1957).
(49) V. Schomaker and L. Pauling, *J. Am. Chem. Soc.*, **61**, 1769 (1939).
(50) GVB CI designates an n–$\pi$ CI for the $n\pi^*$ states and a $\pi$ CI for the $\pi\pi^*$ states.
(51) P. J. Hay and I. Shavitt, *Chem. Phys. Lett.*, **22**, 33 (1973); *J. Chem. Phys.*, **60**, 2865 (1974).
(52) (a) M. A. El-Sayed, *J. Chem. Phys.*, **38**, 2834 (1963); (b) *Acc. Chem. Res.*, **1**, 8 (1968).
(53) J. E. Parkin and K. K. Innes, *J. Mol. Spectrosc.*, **15**, 407 (1965).
(54) R. Scheps, D. Florida, and S. A. Rice, *J. Mol. Spectrosc.*, **44**, 1 (1972).
(55) A. J. Yencha and M. A. El-Sayed, *J. Chem. Phys.*, **48**, 3469 (1968).
(56) The double $\zeta$ calculations[37] verify that the photoelectron assignments are correct.
(57) By $\sigma$ Rydberg orbitals we mean the Rydberg orbitals symmetric with respect to reflection in the molecular plane, i.e., 3s, $3p_y$, $3p_z$, $3d_{yz}$, $3d_{y^2}$, and $3d_{z^2}$. Similarly the $\pi$ Rydberg orbitals are $3p_x$, $3d_{xy}$, and $3d_{xz}$.
(58) W. A. Goddard III, unpublished results.